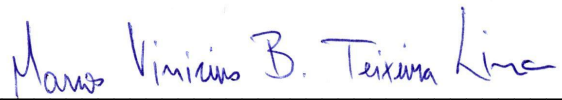


Universidade de São Paulo
Instituto de Física

Oscilações acústicas de bárions no Dark Energy
Survey: detecção no espaço harmônico em
dados do Ano 3

Daniel Charles Heringer Gomes



Orientador: Prof. Dr. Marcos Vinicius Borges Teixeira Lima

Dissertação de mestrado apresentada ao Instituto
de Física como requisito parcial para a obtenção
do título de Mestre em Ciências.

Banca Examinadora:

Prof. Dr. Marcos Vinicius Borges Teixeira Lima (IF-USP)

Prof. Dr. Eduardo Serra Cypriano (IAG-USP)

Prof. Dr. Sandro Dias Pinto Vitenti (UEL)

São Paulo
2022

FICHA CATALOGRÁFICA
Preparada pelo Serviço de Biblioteca e Informação
do Instituto de Física da Universidade de São Paulo

Gomes, Daniel Charles Heringer

Oscilações acústicas de bárions no Dark Energy Survey: detecção no espaço harmônico em dados do Ano 3. São Paulo, 2022.

Dissertação (Mestrado) – Universidade de São Paulo. Instituto de Física. Depto. de Física Matemática.

Orientador: Prof. Dr. Marcos Vinicius Borges Teixeira Lima

Área de Concentração: Cosmologia

Unitermos: 1. Cosmologia; 2. Estrutura do Universo; 3. Escalas de Distâncias.

USP/IF/SBI-014/2022

University of São Paulo
Physics Institute

Baryon acoustic oscillations in the Dark Energy
Survey: harmonic space detection from Year 3
data

Daniel Charles Heringer Gomes

Supervisor: Prof. Dr. Marcos Vinicius Borges Teixeira Lima

Dissertation submitted to the Physics Institute of
the University of São Paulo in partial fulfillment
of the requirements for the degree of Master of
Science.

Examining Committee:

Prof. Dr. Marcos Vinicius Borges Teixeira Lima - Supervisor (IF-USP)

Prof. Dr. Eduardo Serra Cypriano (IAG-USP)

Prof. Dr. Sandro Dias Pinto Vitenti (UEL)

São Paulo
2022

To my parents Davi and Adriana Gomes.

ACKNOWLEDGEMENTS

First of all, I thank the Lord God, Creator of the universe, and praise him for his grace towards us that makes knowledge itself possible.

I express my sincere thanks to my twin brother Rafael Gomes, who worked with me during the whole period of this project, even while performing his own graduate research. I also thank my advisor Dr. Marcos Lima for getting me involved with the Dark Energy Survey collaboration during my time as an undergraduate at USP (which opened the doors for this project to happen) and for always guiding me during the project. I thank Dr. Hugo Camacho for his help in communicating with the collaboration working groups and in understanding their methodology.

I am profoundly grateful to my family, especially my father Dr. Davi Charles Gomes, for shaping my interest in philosophy of science and warning me against the dangers of epistemological naivety in scientific research, and my mother Adriana Gomes, for teaching me mathematics (and so much more) at a very early age. If anything positive and lasting comes from my venture in academic research, they are both responsible for it. I thank my grandfather Dr. Wadislau Martins Gomes for all our conversations about astronomy and cosmology over the years, and my grandmother Elizabeth Gomes for her captivating kindness. Special thanks also go to my uncle Dr. Daniel Gomes, his wife Marcia, and my cousins Davi and Ruth Gomes—they have never been far, even while living on the other side of the world.

Finally, I send my thanks to those friends who were closest to me during the time of this project, namely Samuel Kultz, Giovanna Maringeli, Daniel Kauffman Florentino (with his wife Maria Vitória) and João Vitor Cerqueira. They have all made my life lighter at hard times.

I recognize that this work used the computational facilities of DFMA-IF at the University of São Paulo. Besides that, I was financially supported by CNPq (Conselho Nacional de Desenvolvimento Científico e Tecnológico) for two years, and also benefited from LIneA (Laboratório Interinstitucional de e-Astronomia) as it was responsible for enabling Brazilian participation on DES.

“Any physical theory is always provisional (...). No matter how many times the results of experiments agree with some theory, you can never be sure that the next time the result will not contradict the theory.”

Stephen Hawking

“Curiosity prompts a desire for knowledge, whereas it is only thou who knowest all things supremely.”

Augustine of Hippo

ABSTRACT

In this work, we aim at measuring the angular diameter distance of a given redshift through analysis of baryon acoustic oscillations (BAO) on the angular power spectrum of galaxies captured by the Dark Energy Survey (DES) during its third year of operation. To achieve this goal, we first make a brief review of the history of cosmology, showing the main characteristics and methods of this discipline. We explain the concept of BAO and its relation with cosmological distances. We offer an overview of the Dark Energy Survey experiment, with emphasis on its tomographic BAO detection effort. We present the computational methods used by the DES collaboration on its analysis of Year 3 data, and we show results we obtained from our independent analysis of these data, following the same methodology as the collaboration. We find the value of $D_A(z = 0.835) = 10.36(34)r_s$ for the angular diameter distance, which is compatible with the collaboration's result and has a relative error of the order of 3%. We compare this value with those found by other large cosmological experiments, in order to show how our work takes a step towards better estimates of cosmological parameters.

Keywords: Cosmology. Structure of the Universe. Distance Scales.

RESUMO

Neste trabalho, buscamos medir a distância diâmetro angular de um dado *redshift* através de análise das oscilações acústicas de bárions (BAO) no espectro de potência angular de galáxias fotografadas pelo Dark Energy Survey (DES) em seu terceiro ano de operação. Para cumprir esse objetivo, realizamos primeiro uma breve revisão da história da cosmologia, levantando as principais características e métodos da área. Explicamos o conceito de BAO e sua relação com distâncias na cosmologia. Fornecemos uma visão geral do experimento Dark Energy Survey, com ênfase em seu esforço de detecção tomográfica de BAO. Expomos os métodos computacionais utilizados pela colaboração do DES na análise do terceiro ano de dados do experimento, e mostramos resultados obtidos por nossa análise independente desses dados, seguindo a mesma metodologia da colaboração. Encontramos o valor de $D_A(z = 0.835) = 10.36(34)r_s$ para a distância diâmetro angular, que é compatível com o resultado da colaboração e possui um erro relativo da ordem de 3%. Apresentamos uma comparação desse valor com aqueles obtidos por outros grandes experimentos cosmológicos, a fim de mostrar como nosso trabalho dá um passo em direção a melhores estimativas para os parâmetros cosmológicos.

Palavras-chaves: Cosmologia. Estrutura do Universo. Escalas de Distâncias.

LIST OF FIGURES

Figure 1.1 – William Herschel’s 18 th century map of the universe. Figure from Herschel (1785)	24
Figure 1.2 – Hubble’s plot of the distance-velocity relation. Figure from Hubble (1929)	25
Figure 2.1 – Distance-redshift relation for three different distance measures with MICE and Planck cosmologies.	38
Figure 3.1 – Sky area covered by DES Y1 and Y3 catalogs. Figure from Sevilla-Noarbe et al. (2021)	47
Figure 5.1 – Comparison between theoretical and measured C_ℓ ’s from a single map (identified as f1z1) with $\Delta\ell = 10, 20, 30$	60
Figure 5.2 – χ^2 as a function of the size of multipole bins.	61
Figure 5.3 – Distribution of BAO scale parameter α on the full set of COLA mocks: Histogram with simple gaussian fit.	63
Figure 5.4 – Distribution of BAO scale parameter α on the full set of COLA mocks: Sum of individual probability density functions and a gaussian fit of the sum.	63
Figure 5.5 – BAO scale parameter and scaling factors for MCMC analysis of the mean of COLA mocks.	64
Figure 5.6 – BAO scale parameter and scaling factors for MCMC analysis of Y3 data.	66
Figure 5.7 – DES Y3 measured and best fit angular power spectra.	67
Figure 5.8 – MCMC parameter distribution for redshift dependent analysis of Y3 data.	68
Figure 5.9 – Re-scaled angular diameter distance measurements from recent surveys. Figure from DES Collaboration, Abbott, Aguena, et al. (2021)	69
Figure A.1 – Fitted f_{NL} parameter distribution on the COLA mocks.	88
Figure A.2 – Sampled f_{NL} and bias parameters for different scale cuts.	89

LIST OF TABLES

Table 5.1 – Best fit parameters for two models. Uncertainty values were extracted directly from the covariance matrix given by the optimization code output.	61
Table 5.2 – Best fit parameters for individual and mean data vectors.	64
Table 5.3 – BAO scale parameter measured on Y3 data: Best fit for different pipelines.	65
Table 5.4 – BAO scale parameter for each redshift bin.	68
Table B.1 – Value of all 26 parameters for MLE and MCMC fits with DES Y3 data.	91

CONTENTS

INTRODUCTION	19
1 HISTORICAL AND METHODOLOGICAL OVERVIEW OF COSMOLOGY	23
1.1 THE RISE OF MODERN COSMOLOGY	23
1.1.1 From speculative to scientific cosmology	23
1.1.2 Differences between cosmology and other physical sciences	26
1.1.3 Pragmatic extrapolation	27
1.2 TYPES OF COSMOLOGICAL SURVEYS	28
1.3 METHODOLOGICAL CONCERNS	29
1.3.1 Data fitting with cosmological models	29
1.3.2 Code validation with simulations	30
1.3.3 Blinding	30
2 EXPANSION AND STRUCTURE PATTERNS OF THE UNIVERSE	33
2.1 FROM EINSTEIN EQUATIONS TO AN EXPANDING UNIVERSE	33
2.2 COSMOLOGICAL DISTANCES	37
2.3 2-POINT FUNCTIONS	38
2.3.1 Correlation function and power spectrum	38
2.3.2 The galaxy angular power spectrum	39
2.4 BARYON ACOUSTIC OSCILLATIONS	41
2.4.1 Structure formation and decoupling	41
2.4.2 The BAO scale parameter	42
2.4.3 Non-linear damping of the acoustic signal	42
3 THE DARK ENERGY SURVEY AND ITS BAO EFFORT	45
3.1 THE DARK ENERGY SURVEY	45
3.1.1 History	45
3.1.2 Galaxy Clusters, supernovae and weak lensing	45

3.1.3	Survey camera and footprint	46
3.2	THE BAO EFFORT	46
3.2.1	Year 1 sample characterization	47
3.2.2	Results from Year 1	48
4	METHODS AND SIMULATIONS FOR DARK ENERGY SUR- VEY YEAR 3 ANALYSIS	51
4.1	CODE FOR THE THEORETICAL GALAXY APS	51
4.2	SPECTRUM MEASUREMENTS	52
4.3	MOCK GALAXY CATALOGS	53
4.3.1	COLA	54
4.3.2	FLASK	54
4.4	COVARIANCE	55
4.5	STATISTICS FOR TEMPLATE FITTING	55
4.5.1	Frequentist statistics	56
4.5.2	Bayesian statistics	56
4.6	FINAL MODEL	57
5	RESULTS	59
5.1	FLASK MOCK MEASUREMENTS AND PRELIMINARY TESTS	59
5.1.1	The effect of Δ_ℓ	59
5.1.2	BAO measurement with MLE	61
5.2	COLA MOCK MEASUREMENTS	62
5.3	Y3 DATA ANALYSIS	65
5.3.1	Global fits	65
5.3.2	Redshift dependent fits	65
5.4	ANGULAR DIAMETER DISTANCE	68
	Final Remarks	71
	References	73
	APPENDIX A – PRIMORDIAL NON-GAUSSIANITY TEMPLATES AND PRELIMINARY MEASUREMENTS	85
A.1	CONCEPT	85

A.2	FORMALISM	85
A.2.1	PNG parametrization for the angular power spectra	85
A.2.1.1	A simplified model	87
A.3	PRELIMINARY RESULTS	87
APPENDIX B	– TABLE OF PARAMETERS FOR Y3 MEASURE-	
	MENTS	91

INTRODUCTION

After the first detection of the Baryon Acoustic Oscillations (BAO) signal in the matter distribution of our universe (EISENSTEIN; ZEHAVI, et al., 2005), galaxy survey collaborations have been increasingly interested in results of this type, due to their being a luminosity-independent measurement of cosmological distances. As a consequence, BAO detection has been considered one of the most promising ways of probing information about the history and composition of our universe.

A two-dimensional measurement of the BAO scale can constrain both the angular diameter distance and the Hubble parameter—two independent values useful for probing cosmology. Wagner, C., Müller, V., and Steinmetz, M. (2008) and Shoji, Jeong, and Komatsu (2009) offered different discussions of methods for this double measurement, and were optimistic about the impact of BAO analysis on constraining the dark energy equation of state.

The third program of the Sloan Digital Sky Survey, known as SDSS-III (EISENSTEIN; WEINBERG, et al., 2011), included a spectroscopic survey specifically designed for BAO detection, the BOSS (Baryon Oscillation Spectroscopic Survey). Dawson, Schlegel, et al. (2013) describe this survey as comprising two samples: an extension of the SDSS-I and SDSS-II LRG surveys and a deeper, high redshift incursion. During the following years, SDSS-IV and its extension of the BOSS, known as eBOSS (DAWSON; KNEIB, et al., 2016), contributed more data to this effort.

The rise of these large BAO-directed spectroscopic surveys allowed for two-dimensional measurements of the BAO scale. A final set of eBOSS results, presented by Alam et al. (2021), found constraints of the order of 1% on cosmological parameters combining BAO with other probes.

Photometric surveys have also probed the acoustic feature on galaxy distribution. The Dark Energy Survey (DES), since its beginning, included galaxy angular clustering as one of its analysis fronts (DES COLLABORATION; ABBOTT; ALDERING, et al., 2005). Eventually, a BAO working group was formed, novel analysis methods were devel-

oped inside the collaboration, and results up to the third year of data have already been published (DES COLLABORATION; ABBOTT; AGUENA, et al., 2021).

These developments in BAO detection are an important ingredient in the study of dark energy. The Dark Energy Task Force (ALBRECHT et al., 2006) made forecasts of a quantitative figure of merit for combined dark energy measurements of what they call Stage-III surveys (our current generation—including SDSS-IV and DES). Summing up the results from SDSS-IV, Alam et al. (2021) obtained a slightly smaller figure of merit, but at that time only first year DES results were available. Their prediction is that the original task force forecast value will be achieved after the DES Year 6 analysis is completed.

Our work is situated during the analysis of DES Year 3 data, as a form of independent validation of the collaboration’s methodology for harmonic space BAO analysis. As a member of the collaboration, our goal was to create a code, following the steps of the DES pipeline, to test the mock catalogs used by the collaboration and to measure the BAO scale directly from the DES data.

In order to understand the BAO phenomenon, the theoretical predictions of how it affects the distribution of galaxies in the sky and to test current cosmological models with survey data, we first need to take a step back and look at the rise of cosmology during the twentieth century, which led to the idea of large cosmological surveys. This is needed to establish exactly the objective, effectiveness and limitations of these surveys, since they generate the data which we have studied.

We will start, in Chapter 1, with this brief overview of cosmology, followed by a theoretical modeling of the universe as a whole (Chapter 2). In Chapter 3, we will visit the basic characteristics of the Dark Energy Survey and of its Year 1 samples and methodologies.

Our programming work, using the theoretical baggage from Chapter 2, will be discussed in Chapter 4, together with a description of the mock catalogs we used for testing our code and for preliminary results. Chapter 5, finally, will show our numeric results, starting from short tests done during the beginning of the project, passing through BAO measurements on simulations, and culminating in a BAO measurement from DES data.

On Appendix A, we will briefly describe a side project we developed during our time at USP, where we adapted our codes to function as a primordial non-gaussianities detection pipeline. This is an ongoing project, and only preliminary results will be shown.

HISTORICAL AND METHODOLOGICAL OVERVIEW OF COSMOLOGY

1.1 THE RISE OF MODERN COSMOLOGY

1.1.1 From speculative to scientific cosmology

Cosmology as a science is a recent endeavor, which began early in the twentieth century, with the rise of distance measuring methods for astronomical objects. Before distances to celestial bodies could be determined, only projected maps could be drawn. This means the observed objects could be anywhere; and consequently, of any size.

In this context, speculative cosmologies were ways of proposing somewhat philosophical models to account for what appeared in the night sky. Thinkers such as Descartes and Kant wrote their own takes on the structure of the universe at a time where there still weren't methods to test these ideas (LONGAIR, 2004). During the 18th century, William Herschel mapped the known objects he observed, assuming brightness of stars as a measure of distance (this works if it is presupposed that all stars have equal absolute brightness). His proposed chart is shown on Figure 1.1, and it represents a small bounded universe, with all stars within the observer's reach. According to Longair (2004), Herschel's project was the first quantitative model of the size of the universe.

In the first half of the 19th century, distance measurements through stellar parallax started to yield results (SIDOLI, 2021), which paved the way for an empirical three-dimensional concept of the sky. The great advance that established the modern notion of the universe (as something not limited to the Milky Way, but rather composed by an enormous amount of objects of its type) happened already in the twentieth century: it was Edwin Hubble's observation of Cepheid stars in the Andromeda Galaxy. This kind of variable stars have a strict relation between their period and their absolute luminosity, discovered by Henrietta Leavitt (FREEDMAN; MADORE, 2010; LEAVITT; PICKERING, 1912). Therefore, the distance to Andromeda could be determined, to the point

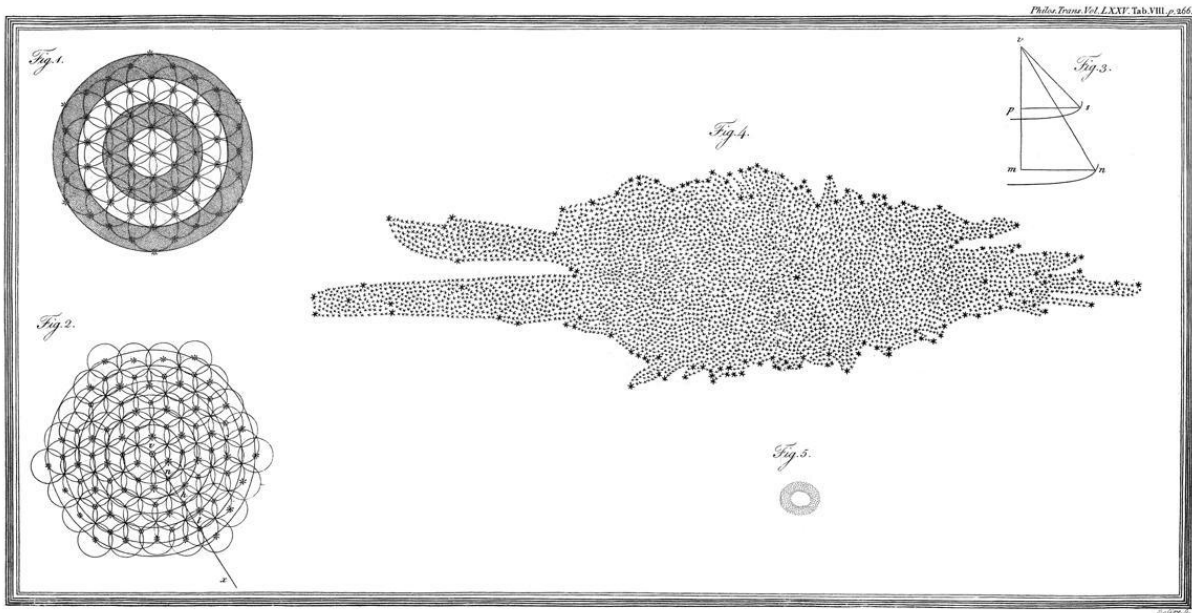


Figure 1.1 – William Herschel’s 18th century map of the universe. Figure from [Herschel \(1785\)](#)

that it was seen to be much greater than the known size of the Milky Way. This settled an ongoing debate and allowed for the rise of scientific cosmology.

The other ingredient necessary for modeling our universe was Einstein’s theory of general relativity. As an understanding of the structure of space-time, it was rapidly applied to the universe as a whole, and not without debate, astronomers finally used it to sustain the idea of a dynamic universe, currently expanding. In 1929, observations of Cepheids on several galaxies gave Hubble a set of distance measurements that allowed him to establish an empirical distance-velocity relation (see Eq. 1.1, Figure 1.2) ([BAHCALL, 2015](#)).

$$v = H_0 \times d \quad (1.1)$$

This relation became known as the Hubble Law¹, and was clear evidence of the expansion of the universe, thus marking the beginning of cosmology as an independently defined field of research. Though the debate around the universe as eternal or expanding from a beginning event was still fervent during the following decades, the debate itself already worked to show that cosmology would develop as essentially a historical science: If one expects to predict structure in the universe and test predictions from data, these tests would necessarily require a physical modeling of the dynamics of the universe throughout the past.

¹ Recently renamed as the Hubble-Lemaître law.

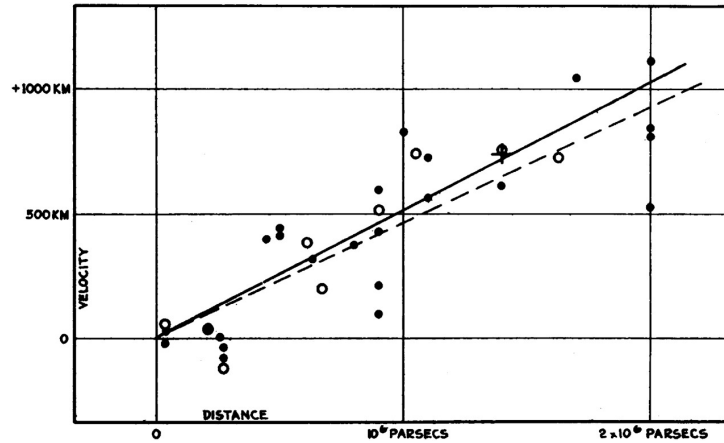


Figure 1.2 – Hubble’s plot of the distance-velocity relation. Figure from [Hubble \(1929\)](#)

During the 1960s, a main prediction of models where the universe expands from a single beginning event was experimentally confirmed by Arno Penzias and Robert Wilson ([LONGAIR, 2004](#)). They measured a radiation signal with the same temperature as the theoretically proposed Cosmic Microwave Background (CMB)—a relic of the moment when light would have decoupled from matter in an expanding universe. From this discovery forward, cosmology has basically relied on expansion models. Certain initial conditions are assumed for the universe at a moment immediately after the beginning². Then, Einstein’s framework is used to predict how this expansion would take place until a distribution of matter similar to the one we observe is achieved.

The following years have seen these theoretical studies walk side by side with technological improvements in observational astronomy. Large galaxy and CMB surveys changed the face of cosmology, with large amounts of data being generated and checked against theory—this became known as the era of precision cosmology. Currently, the most well-accepted model for the universe is known as Λ CDM: It considers a General Relativity framework with cold dark matter and a constant Λ , often called dark energy, inserted so that the recently detected accelerating expansion can be explained.

The measurement of features of our universe is still expected to produce changes in the way we describe it, changes which can involve new descriptions of physical entities or even structurally modifying the previously used physical models ([LAHAV; MASSIMI, 2014](#)).

² A scientific model essentially presupposes the existence of that which it describes. In this sense, a description of the beginning event itself escapes the realm of scientific investigation, becoming a metaphysical issue

1.1.2 Differences between cosmology and other physical sciences

Having seen how the field of scientific cosmology was established, we proceed to highlight a significant conceptual distinction between this discipline and other physical sciences. Ellis (2006) introduces this issue by remembering us that

we cannot alter [the initial conditions of the universe] (...) in any way —they are given to us as absolute and unchangeable, even though they are understood as contingent rather than necessary; that is, they could have been different while still being consistent with all known physical laws. (ELLIS, 2006, p. 1216)

According to Ellis, there are two main consequences that follow this affirmation. First, there is the distinction between usual experimental sciences and historical sciences. While the former deal with objects and events that can be measured and recreated, the latter investigates the past, having therefore a more observation-based character. The fact that there is only one past imposes an intrinsic methodological limitation to these sciences, for the methods of experimentation need to rely on what is already there, and infer the past based on those results.

A second limitation, which makes cosmology different even from the other historical sciences, is that the object of inquiry —the universe —has nothing similar to be compared to. Astrophysicists, when dealing with the origin of a planet, a star or a galaxy, have other objects of the same kind to extract general rules and models. A cosmologist, however, does not have access to other universes with different behaviors. Therefore, the concept of a general law is hard to be defined, as a law is usually defined through generalization (ELLIS, 2006).

Because of that, an explanatory model for the history of the universe cannot be tested with data from the actual sky alone. It is necessary to have parameters where different values render different outputs, and some way of testing the possible predictions against the real universe. The solution eventually found was that cosmology would become extremely dependent on simulations. Technological development allowed physicists to create mock catalogs, similar to those created with data from telescopes, but generated with a large range of theoretical models and parameters.

When dealing with simulated universes, we need to keep in mind that they are essentially partial: no one has exhaustive knowledge of the universe, so a simulation only reproduces a specific set of known objects and phenomena (ELLIS, 2006). Therefore, we

have to think critically about cosmological results, taking special care to the fact that our model preferences rely on the choices and presuppositions present when the simulations and models were developed.

1.1.3 Pragmatic extrapolation

During the first decades of experimental cosmology, certain properties or physical models were assumed to be true, though without any way of assessing their validity, so that analysis could take place. [P.J.E. Peebles \(2020\)](#), reflecting on the development of cosmology from this initial state until the age of large surveys, says these assumptions were “pragmatic extrapolations”—scientists had to believe the same physics of small astronomical scales was applicable to the universe as a whole. The greatest example stressed by Peebles is that General Relativity applies to the largest scales of the universe.

Developing theoretical predictions based on these assumptions ended up being the way forward and, as expected, new observations eventually arose to support them. Two of them are mentioned, both happening near the turn of the century: The mapping of CMB anisotropies by WMAP and its constraints on cosmological parameters ([SPERGEL et al., 2003](#)) and the establishment of distance-redshift relations through the magnitude of Type Ia supernovae, that function as standard candles. According to [P.J.E. Peebles \(2020\)](#), the relevance of these results is that they were independent tests of a same model, that would not be expected to agree if this model was strongly flawed.

Today, we have a clear inferred history of the universe, grounded on the Λ CDM model, and though it may not be a satisfactory or true description of what happened, it best matches the data than any other idea proposed up to now.

This does not mean that modern cosmology has no fundamental challenges. The initial challenges of the Big Bang, which eventually led to the idea of inflation, are, according to some cosmologists, still unaccounted for by the inflationary framework. Besides that, the fact that our account of cosmology relies largely on unknown entities, such as dark energy, shows clearly how it is at least incomplete ([ZYLA et al., 2020](#)). The effort of 21st century cosmology is exactly to try to establish a more faithful account of our history.

This end goal, however, still looks far from reach. Currently, large sky surveys are increasing in depth, range and precision but the data we have can only constrain cosmological parameters to a current extent. The next decades will be crucial as the technology

for improved sky maps is being consolidated. We believe theoretical suggestions will have to accompany such development proposing new questions to be asked to the data.

Our work in a sky survey collaboration, therefore, does not expect to solve the great problems of cosmology. It serves, however, as a small step in this process, training scientists with the analytical tools necessary for the next generation of cosmological research, and maybe providing small insights regarding where the research community should direct its efforts.

1.2 TYPES OF COSMOLOGICAL SURVEYS

A sky survey should be able to constrain the three-dimensional position of the surveyed objects. While their angular position is trivially determined, the distance cannot be directly measured. The relation between distance and redshift allows us to approach this problem as the issue of acquiring precise redshift measurements.

In order to find the redshift of a galaxy, its spectrum can be measured and compared with expected galaxy spectra—this is the concept of a spectroscopic survey (DJORGOVSKI *et al.*, 2013). This kind of sky survey has the advantage of getting precise redshift values, at the cost of having to detect the spectral lines instead of a simple luminosity measurement. A photometric sky survey is a survey that measures solely the light intensity at a small amount of bands. This allows the survey to include a larger amount of galaxies, but the redshift determination becomes harder, since less information is preserved. A redshift value from a photometric survey is known as a photometric redshift (photo- z).

The first methods for photo- z estimation to be explored were template methods, where the luminosity on the measured bands was compared to some template data with known spectroscopic redshifts. Galaxies with similar luminosity distribution between the bands were assumed to have similar redshifts. For this kind of method, the size and representativity of the template catalog are crucial to minimize the errors (COLLISTER; LAHAV, 2004). A second kind of photo- z estimation process is to try to establish a mathematical relation between the luminosity input and the known spectroscopic redshift of several galaxies, extrapolating the result to the galaxies where there is no spectroscopic measurement. This concept is best applied with the use of neural networks, because they allow complex parameterizations which can be always improved with new training sets. Some have suggested methods that estimate directly the redshift distribution of a sample

instead of performing estimates for each individual galaxy (see the forward modeling approach by [Herbel et al. \(2017\)](#)).

Photometric redshifts, being produced by an empirical process, have wide probability distribution functions, and are not so useful as individual measurements of specific objects. Still, these errors can be dealt with when working with large galaxy catalogs, by means of combining galaxies within a similar redshift range. All data is divided into redshift bins and projected onto slices with an average redshift value. This removes the radial dimension, and all radial positions are treated only on the moment where the galaxies are assigned to a single redshift bin. This process, as it deals with projected two-dimensional maps, is called a tomographic analysis.

Two types of correlation functions can be defined on these two-dimensional maps: autocorrelation functions, using pairs of galaxies from the same redshift bin; and cross-correlation functions, where pairs are formed with one galaxy from a specific redshift bin and the other from a second one. The latter establishes the correlation between the position of galaxies of the two different redshift bins. The precise mathematical definition of these functions will be presented in [Section 2.3](#).

1.3 METHODOLOGICAL CONCERNS

Before we move towards our theoretical overview, some general concerns need to be stressed regarding the way survey data is used to probe cosmology.

1.3.1 Data fitting with cosmological models

Our first methodological concern is related to the way information can be extracted from sky images. Cosmological models show how each set of parameters would be responsible for a universe with different features. In order to numerically constrain these parameters, we need mathematical functions to measure the specific features we are looking for. These functions serve as the main object of research, and are explored through theoretical models and measured from sky images so that both can be compared.

To pick a specific function is to preserve a specific part of the information collected by the survey. Therefore, the selection of the function itself must be conscious in terms of which choice would give more precise determinations of the desired parameters. A recent

example of efforts to diversify function selection in order to preserve information is the procedure described by [Neyrinck, Szapudi, and Szalay \(2009\)](#).

1.3.2 Code validation with simulations

As we have anticipated when characterizing cosmology, the use of simulations of the universe is essential to validate developed methodology before it can be applied to actual data. During this process, one has to keep in mind both that mock data is always controlled, generated to mimic specific features, and therefore prone to error when dealing with unknown features. In this sense, extensive robustness testing has to be done to see if the desired methodology can actually work for a wide range of possible universes, not only those akin to the simulated environment.

1.3.3 Blinding

Differently from the two previous concerns, our last one is more related to the philosophical foundations of the scientific process, and is often misunderstood by those whose research focus is solely on the mathematical and computational processes in data analysis. We will start addressing this issue with the question: Do our preconceived models or expectations in cosmology affect the elaboration of analysis methods? There is no doubt that the answer is affirmative. Confirmation bias is a well known problem in science, and an area of study which relies on a single picture of reality (apart from simulations) is specifically prone to this tendency.

[Croft and Dailey \(2015\)](#) analyze cosmological parameter measurements throughout the years and show how there is an inaccurate tendency of favoring specific values. Looking at the case of Ω_Λ measurements, the authors suggest that both overestimated errors and confirmation bias might be in the play.

A well known solution to minimize this effect is the process of blinding. Cosmological data analysis collaborations have used this process since 2006 ([MUIR et al., 2020](#); [CONLEY et al., 2006](#)), and today blinded analyses are considered of much stronger value than unblinded ones.

Blinding is, essentially, a strategy of limiting the scientist's knowledge of the data during the analysis process, and can be done directly on the raw data from surveys or on the measured functions. Scientists which work with blinded data or blinded correlation

functions do not have access to the original material, so their results are not expected to be the true ones, though blinding cannot shift them too far that eventual problems with the data would not be detected. The idea is to transform the object of analysis to a point that it still can be used to gather insights on systematic effects, but has less power to induce bias in terms of the final numerical result.

The Dark Energy Survey (DES) has implemented blinding strategies on both catalog and parameter level, besides avoiding plots which could provoke a visual bias (this can be done by not showing values on the axes and not performing some explicit comparisons with theory) ([TROXEL et al., 2018](#)).

EXPANSION AND STRUCTURE PATTERNS OF THE UNIVERSE

2.1 FROM EINSTEIN EQUATIONS TO AN EXPANDING UNIVERSE

We now move to a brief review of the theoretical concepts to be used in our analysis. The equations that determine the dynamics of our universe are a consequence of Einstein's general relativity equation (DODELSON, 2003).

$$R_{\mu\nu} - \frac{1}{2}g_{\mu\nu}\mathcal{R} = 8\pi GT_{\mu\nu} \quad (2.1)$$

where the Ricci tensor $R_{\mu\nu}$ is a contraction of the first and third indices of the Riemann tensor, defined by Eq. 2.2 (SCHUTZ, 2009),

$$R^{\mu}_{\nu\rho\sigma} = \Gamma^{\mu}_{\nu\sigma;\rho} - \Gamma^{\mu}_{\nu\rho;\sigma} + \Gamma^{\mu}_{\lambda\rho}\Gamma^{\lambda}_{\nu\sigma} - \Gamma^{\mu}_{\lambda\sigma}\Gamma^{\lambda}_{\nu\rho}, \quad (2.2)$$

with the Christoffel symbols

$$\Gamma^i_{jk} = \frac{g^{i\nu}}{2} \left(\frac{\partial g_{j\nu}}{\partial x^k} + \frac{\partial g_{k\nu}}{\partial x^j} - \frac{\partial g_{\nu k}}{\partial x^j} \right). \quad (2.3)$$

As we have previously stated, we assume general relativity is valid when dealing with the dynamics of the universe as a whole. We also take the universe to be homogeneous and isotropic in large scales. Then, we consider the metric tensor in an open universe with curvature density Ω_k , where a is the time-dependent scale factor, related to the redshift through Eq. 2.4.

$$a = \frac{1}{(1+z)}. \quad (2.4)$$

The metric is written on standard spherical coordinates:

$$g_{\mu\nu} = \begin{bmatrix} -1 & 0 & 0 & 0 \\ 0 & \frac{a^2}{1+\Omega_k H_0^2 r^2} & 0 & 0 \\ 0 & 0 & a^2 r^2 & 0 \\ 0 & 0 & 0 & a^2 r^2 \sin^2 \theta \end{bmatrix}. \quad (2.5)$$

We compute the tensors involved in Einstein's equation, and then work through its time component.

The Christoffel symbols Γ^i_{jk} can be written for the following cases.

- For $i = 0$:

$$\Gamma^0_{jk} = \frac{g^{0\nu}}{2} \left(\frac{\partial g_{j\nu}}{\partial x^k} - \frac{\partial g_{kj}}{\partial x^\nu} + \frac{\partial g_{\nu k}}{\partial x^j} \right). \quad (2.6)$$

We can easily notice that the only non-zero term is the one with $\nu = 0$, because of the $g^{0\nu}$ factor. On this case, the first and last terms on the parenthesis will equal zero. The remaining term, $-\partial g_{kj}/\partial x^\nu$, will equal zero only if $j = 0$ or $k = 0$. Thus, we have:

$$\Gamma^0_{00} = \Gamma^0_{j0} = \Gamma^0_{0k} = 0, \quad (2.7)$$

$$\Gamma^0_{jk} = -\frac{1}{2} \left(-2\frac{\dot{a}}{a}g_{jk} \right) = g_{ij}H \quad (2.8)$$

where $H = \dot{a}/a$ is known as the Hubble factor.

- For $i \neq 0$ and $j = 0$:

$$\Gamma^i_{0k} = \frac{g^{i\nu}}{2} \left(\frac{\partial g_{0\nu}}{\partial x^k} - \frac{\partial g_{k0}}{\partial x^\nu} + \frac{\partial g_{\nu k}}{\partial x^0} \right). \quad (2.9)$$

The only non-zero term, on this case, will be $\nu = i$. On this case, if $k = 0$, all the terms on the parenthesis will also equal zero. If $k \neq 0$, the last term remains. Thus, we have:

$$\Gamma^i_{00} = 0, \quad (2.10)$$

$$\Gamma^i_{0k} = \frac{1}{2g_{ii}} \left(2\frac{\dot{a}}{a}g_{ik} \right) = \delta^i_k H. \quad (2.11)$$

- For $i \neq 0$, $j \neq 0$ and $k = 0$:

This case can be solved in the same way as the previous one. We obtain:

$$\Gamma^i_{j0} = \frac{1}{2g_{ii}} \left(2\frac{\dot{a}}{a}g_{ji} \right) = \delta^i_j H. \quad (2.12)$$

- For $i \neq 0$, $j \neq 0$ and $k \neq 0$, we keep the form of Eq. 2.3.

From Eq. 2.2, the Ricci tensor is:

$$R_{\mu\nu} = \frac{\partial \Gamma^\lambda_{\mu\nu}}{\partial x^\lambda} - \frac{\partial \Gamma^\lambda_{\mu\lambda}}{\partial x^\nu} + \Gamma^\eta_{\mu\nu} \Gamma^\lambda_{\lambda\eta} - \Gamma^\eta_{\mu\lambda} \Gamma^\lambda_{\nu\eta}. \quad (2.13)$$

Therefore, its 00 component is:

$$R_{00} = \frac{\partial \Gamma^\lambda_{00}}{\partial x^\lambda} - \frac{\partial \Gamma^\lambda_{0\lambda}}{\partial x^0} + \Gamma^\eta_{00} \Gamma^\lambda_{\lambda\eta} - \Gamma^\eta_{0\lambda} \Gamma^\lambda_{0\eta} \quad (2.14)$$

$$\Rightarrow R_{00} = -3 \frac{dH}{dt} - 3H^2 = -3 \left(\frac{\ddot{a}}{a} - \left(\frac{\dot{a}}{a} \right)^2 \right) - 3 \left(\frac{\dot{a}}{a} \right)^2 \quad (2.15)$$

$$\Rightarrow R_{00} = -3 \frac{\ddot{a}}{a}. \quad (2.16)$$

The spatial components can also be found through Eq. 2.13. For each case, we use the Christoffel symbols we had previously obtained, summing over the λ and η indices. We get:

$$i \neq j \quad \Rightarrow \quad R_{ij} = 0. \quad (2.17)$$

$$R_{11} = \frac{a\ddot{a} + 2\dot{a}^2}{1 + \Omega_k H_0^2 r^2} - \frac{2}{r} \frac{\Omega_k H_0^2 r}{1 + \Omega_k H_0^2 r^2} = \frac{a\ddot{a} + 2\dot{a}^2 - 2\Omega_k H_0^2}{1 + \Omega_k H_0^2 r^2} \quad (2.18)$$

$$\Rightarrow R_{11} = \frac{a^2}{1 + \Omega_k H_0^2 r^2} \left(\frac{\ddot{a}}{a} + 2H^2 - \frac{2\Omega_k H_0^2}{a^2} \right). \quad (2.19)$$

$$R_{22} = 2r^2 \dot{a}^2 + r^2 a \ddot{a} - 2\Omega_k H_0^2 r^2 \quad (2.20)$$

$$\Rightarrow R_{22} = a^2 r^2 \left(\frac{\ddot{a}}{a} + 2H^2 - \frac{2\Omega_k H_0^2}{a^2} \right). \quad (2.21)$$

$$R_{33} = (a\ddot{a} + 2\dot{a}^2) r^2 \sin^2 \theta - 2\Omega_k H_0^2 r^2 \sin^2 \theta \quad (2.22)$$

$$\Rightarrow R_{33} = a^2 r^2 \sin^2 \theta \left(\frac{\ddot{a}}{a} + 2H^2 - \frac{2\Omega_k H_0^2}{a^2} \right). \quad (2.23)$$

Therefore, we can write a general expression for this results, in terms of the common factor that appeared. We obtain:

$$R_{ij} = g_{ij} \left(\frac{\ddot{a}}{a} + 2H^2 - \frac{2\Omega_k H_0^2}{a^2} \right). \quad (2.24)$$

The Ricci scalar is given by:

$$\mathcal{R} = g^{\mu\nu} R_{\mu\nu}. \quad (2.25)$$

From the components we have computed, we find:

$$\mathcal{R} = 3\frac{\ddot{a}}{a} + 3\left(\frac{\ddot{a}}{a} + 2H^2 - \frac{2\Omega_k H_0^2}{a^2}\right) \quad (2.26)$$

$$\Rightarrow \mathcal{R} = 6\left(\frac{\ddot{a}}{a} + H^2 - \frac{\Omega_k H_0^2}{a^2}\right). \quad (2.27)$$

Replacing these results in Eq. 2.1, for the time-time component, we obtain

$$-3\frac{\ddot{a}}{a} + 3\left(\frac{\ddot{a}}{a} + H^2 - \frac{\Omega_k H_0^2}{a^2}\right) = 8\pi G\rho \quad (2.28)$$

$$\Rightarrow 3\left(H^2 - \frac{\Omega_k H_0^2}{a^2}\right) = 8\pi G\rho \quad (2.29)$$

$$\Rightarrow \left(\frac{\dot{a}}{a}\right)^2 - \frac{\Omega_k H_0^2}{a^2} = \frac{8\pi G\rho}{3} \quad (2.30)$$

$$\Rightarrow \left(\frac{\dot{a}}{a}\right)^2 = \frac{8\pi G\rho}{3} + \frac{\Omega_k H_0^2}{a^2}. \quad (2.31)$$

For a universe with matter, radiation and dark energy, the density breaks up into $\rho = \rho_m a^{-3} + \rho_r a^{-4} + \rho_{DE} a^{-3(1+w)}$ (each term corresponding to each entity respectively).

$$\left(\frac{\dot{a}}{a}\right)^2 = \frac{8\pi G(\rho_m a^{-3} + \rho_r a^{-4} + \rho_{DE} a^{-3(1+w)})}{3} + \frac{\Omega_k H_0^2}{a^2}. \quad (2.32)$$

In terms of density parameters defined as $\Omega = 8\pi G\rho/(3H_0^2)$,

$$\left(\frac{\dot{a}}{a}\right)^2 = H_0^2(\Omega_m a^{-3} + \Omega_r a^{-4} + \Omega_{DE} a^{-3(1+w)}) + \frac{\Omega_k H_0^2}{a^2} \quad (2.33)$$

$$\Rightarrow \left(\frac{\dot{a}}{a}\right)^2 = H_0^2(\Omega_k a^{-2} + \Omega_m a^{-3} + \Omega_r a^{-4} + \Omega_{DE} a^{-3(1+w)}). \quad (2.34)$$

Eq. 2.34 is the Friedmann Equation for a universe with matter, radiation, dark energy and curvature, and models the evolution of our universe as a whole. The left side of this equation can be written in terms of the Hubble factor as H^2 .

2.2 COSMOLOGICAL DISTANCES

An expanding universe, such as the one described by the Friedmann Equation, can have different distance rulers, depending on how distance is defined. Three main distances measures are commonly used. The comoving distance is the integral of the infinitesimal distance $\delta D(z)/(1+z)$, where the $1+z$ factor is introduced to correct for the difference between the scale factor now and when the object was detected (HOGG, 1999). We have:

$$D_C(z) = c \int_0^z \frac{dz'}{H(z')} \quad (2.35)$$

This measure works for the line-of-sight distance, but needs a correction when measuring transverse distances if the curvature is non-zero. Hogg (1999) shows the transverse comoving distance as

$$D_M(z) = \begin{cases} \frac{c}{H_0\sqrt{\Omega_k}} \sinh \frac{D_C(z)H_0\sqrt{\Omega_k}}{c} & \text{if } \Omega_k > 0 \\ D_C(z) & \text{if } \Omega_k = 0 \\ \frac{c}{H_0\sqrt{|\Omega_k|}} \sin \frac{D_C(z)H_0\sqrt{|\Omega_k|}}{c} & \text{if } \Omega_k < 0 \end{cases} \quad (2.36)$$

The angular diameter distance is the trigonometrical measurement of the distance one gets when using the angular diameter of an object and comparing it with its actual physical size. It is given by

$$D_A(z) = \frac{D_M(z)}{1+z}. \quad (2.37)$$

Finally, the luminosity distance is the one that related apparent and absolute magnitudes, and it can be written as

$$D_L(z) = (1+z)D_M(z). \quad (2.38)$$

The two previous relations (Eqs. 2.37 and 2.38) are demonstrated by Weinberg (1972). He further concludes that, since the three distance measurements differ only by factors of $1+z$, if one has a precise determination of the redshift, a single probe is needed for the distance.

Precise distance measurements can be a way of constraining cosmological parameters. From Eq. 2.35 it can be seen that the comoving distance depends on the Hubble factor, which evolves differently for each set of cosmological parameters (See Eq. 2.34).

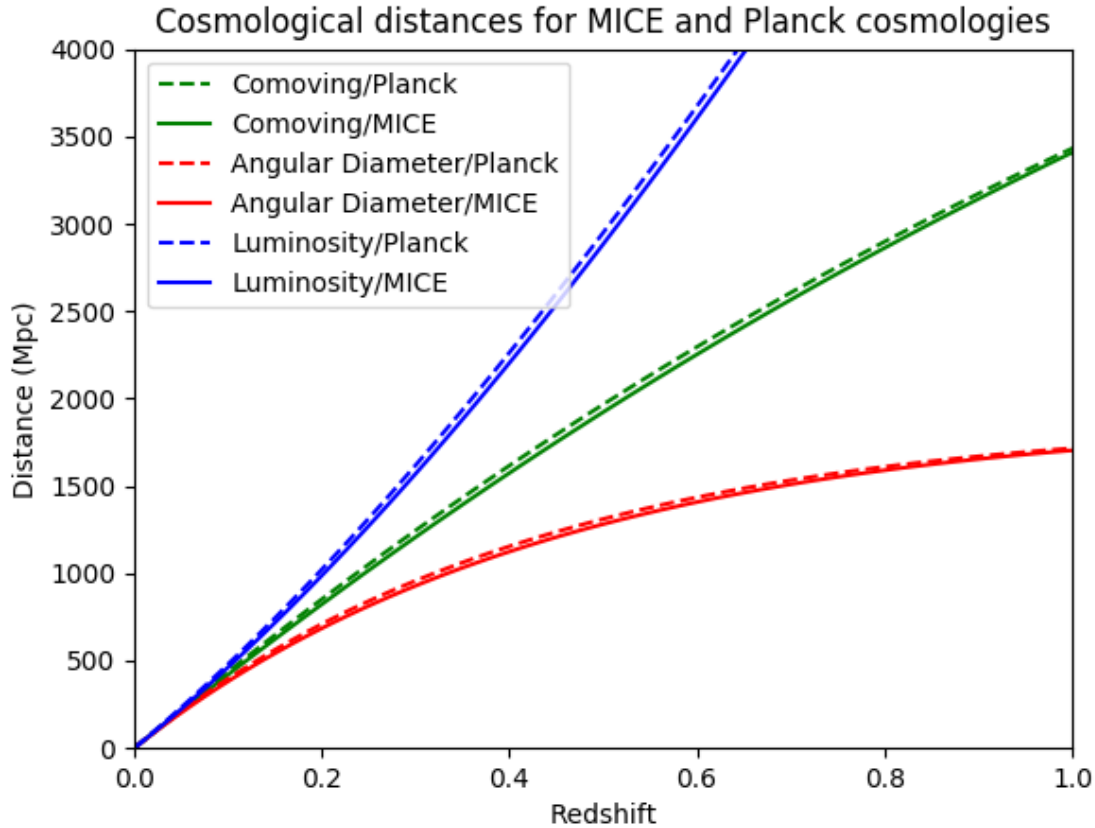


Figure 2.1 – Distance-redshift relation for three different distance measures with MICE and Planck cosmologies.

Figure 2.1 shows the three distance measures as functions of the redshift for two common cosmologies: The one used to create the MICE *Grand Challenge* simulation (FOS-ALBA et al., 2015) and the cosmological parameters determined by the Planck experiment (PLANCK COLLABORATION et al., 2020). MICE cosmology has $\Omega_m = 0.25$, $\Omega_\Lambda = 0.75$, $H_0 = 70(Km/s)/Mpc$; and Planck, $\Omega_m = 0.31$, $\Omega_\Lambda = 0.69$, $H_0 = 67.4$. Though small, the difference clearly reflects on distance measurements.

2.3 2-POINT FUNCTIONS

2.3.1 Correlation function and power spectrum

The spatial distribution of the contents of the universe can be measured by statistical functions. A 2-point function deals with statistics of sets of two different points on the universe, and it can give insight on how the universe is structured on the large scale. The 2-point correlation function $\xi(r)$ measures the distribution of points separated by a

specific distance r . It is defined by Eq. 2.39 (BOSCH, 2020).

$$\xi(\vec{r}) = \langle \delta(\vec{x})\delta(\vec{x} + \vec{r}) \rangle \quad (2.39)$$

The Fourier transform of the correlation function is called the power spectrum.

$$P(\vec{k}) = \int d^3\vec{r} \xi(\vec{r}) e^{-i\vec{k}\vec{r}} \quad (2.40)$$

As the matter distribution of the universe evolves, changes in matter distribution affect the power spectrum. Its evolution can be written as

$$P(k, z) \propto T(k)^2 D(z)^2 \quad (2.41)$$

where $T(k)$ is called the transfer function and $D(z)$ the growth function (DODELSON, 2003). The growth function measures the re-scaling of the spectrum with redshift; and the transfer function tells us how the particular physical interaction between different components of the universe affect the initial perturbations (EISENSTEIN; HU, 1998).

2.3.2 The galaxy angular power spectrum

The angular power spectrum (APS) is a two-dimensional projection of the power spectrum, used for tomographic data analysis. To define the galaxy angular power spectrum, we begin with the galaxy overdensity δ_g , defined as

$$\delta_g(\vec{x}) = \frac{n_g(\vec{x}) - \bar{n}_g}{\bar{n}_g} \quad (2.42)$$

This overdensity can be modeled as the matter overdensity multiplied by a linear galaxy bias. Since we want 2D-functions, this overdensity has to be projected on redshift shells. This projected overdensity will be denoted as δ_g^i , where i indicates the redshift bin.

When we expand δ_g^i on spherical harmonics, the APS is the expected value of the expansion coefficients $a_{\ell m}^i$. The following expression (CAMACHO et al., 2019) defines the APS (for correlations within the same bin, $i = j$) and the cross spectrum (for $i \neq j$). Although we will show the theory for this general case, we will only work with auto-correlations.

$$\langle a_{\ell m}^i (a_{\ell' m'}^j)^{j*} \rangle = \delta_{\ell\ell'} \delta_{mm'} C_\ell^{ij} \quad (2.43)$$

In order to compute the C_ℓ 's, we have to perform two integrals, the projection on redshift shells and the spherical harmonic transform. Starting with the power spectrum $P(k)$ at redshift zero, we have (CAMACHO et al., 2019; SOBREIRA et al., 2011):

$$C_\ell^{ij} = \int_0^\infty dk k^2 P(k) \psi_\ell^i(k) \psi_\ell^j(k) \quad (2.44)$$

where

$$\psi_\ell^i(k) = \sqrt{\frac{2}{\pi}} \int_0^\infty dz W_g^i(z) j_\ell(kr(z)) + R_\ell^i(k) \quad (2.45)$$

On Eq. 2.45, the last term includes the redshift space distortions, which will not be taken into account for our project. As for the other terms, j_ℓ are the spherical Bessel functions, and $W(z)$ is the window function

$$W_g^i(z) = \phi_g^i(z) b_g(z) G(z) \quad (2.46)$$

Here, ϕ_g^i is the selection function, b_g is the galaxy bias and $G(z)$ is the normalized growth function

$$G(z) = \frac{D(z)}{D(z=0)} \quad (2.47)$$

A common way of simplifying these calculations is using the Limber approximation (LOVERDE; AFSHORDI, 2008; CHAVEZ, 2014), which transforms the double integral into a single integral. It is given by Eq. 2.48, and it is known to be a good approximation for the scales of our interest ($\ell > 50$).

$$C_\ell^{ij} = \int_0^\infty dz \frac{W_g^i(z) W_g^j(z)}{r(z)^2} P\left(\frac{\ell + 1/2}{r(z)}\right) \quad (2.48)$$

The Limber approximation gives us a relation between the scale k and the multipole ℓ , which can be useful when comparing the location of specific features in both spectra. This relation is shown on Eq. 2.49, and it will be used later in order to determine the scale cuts for our analysis on each redshift bin.

$$k = \frac{\ell + 1/2}{r(z)} \quad (2.49)$$

2.4 BARYON ACOUSTIC OSCILLATIONS

2.4.1 Structure formation and decoupling

The next step towards the characterization of measurable functions is to deal with the formation of the structure patterns in the universe given its background expansion. There is an extensive theoretical modeling based on perturbation theory to treat how initial density perturbations can grow up to generate observable patterns on the modern-day universe.

As general relativity relates the energy-momentum tensor with the metric, density perturbations will always correspond to perturbations in the metric. These perturbations can be of three types: scalar, vector and tensor. Scalar perturbations are related to Newtonian gravity, they determine the interaction of matter density and pressure perturbations; vector perturbations correspond to velocity ones; and tensor perturbations, to gravity waves (KURKI-SUONIO, 2020). Therefore, to our problem of structure formation, scalar perturbations are the most relevant.

Ma and Bertschinger (1995) and Knobel (2013) both offer full analytical demonstrations of the effect of these perturbations. Baryonic matter, today, behaves similarly to dark matter, following its gravitational pull. However, at the early universe, the effect of radiation moved baryons outward, generating a pattern that still can be seen as a relic on the sky. The pattern we see reflects a frozen image of the baryon distribution from the time of decoupling.

During the first stages of the development of our universe, when temperatures were still sufficiently high, photons and baryons were in a tightly coupled state. The photon-baryon fluid, therefore, was subject to the radiation pressure of the photons and the gravitational attraction of baryons, and this led perturbations on the fluid to propagate as acoustic waves, known as baryon acoustic oscillations (BAO). As the temperature decreased, the mean free path of photons increased until they decoupled from baryons, freezing the peak of the acoustic waves at a specific distance from the initial perturbation, which corresponds to the sound horizon at the time of decoupling. This distance, therefore, became a characteristic scale of the matter distribution of the universe and of the CMB.

If we use the two-point correlation function to describe the CMB or the clustering of galaxies, a characteristic scale of distribution appears as a single peak on the function.

When working with power spectra, this peak manifests itself as a series of oscillations. Both frameworks can be used on BAO research.

2.4.2 The BAO scale parameter

The sound horizon at the decoupling redshift z_d is given by

$$r_s = \int_{z_d}^{\infty} dz \frac{c_s(z)}{H(z)}, \quad (2.50)$$

where the sound speed is given by

$$c_s(z) = \frac{c}{\sqrt{3[1 + R(z)]}}, \quad (2.51)$$

and

$$R(z) = \frac{3\Omega_b(1+z)^3}{4\Omega_r(1+z)^4}. \quad (2.52)$$

The BAO scale r_s , when observed in galaxy correlations at redshift z_g , defines a peak at the BAO angular scale θ_{BAO} :

$$\theta_{\text{BAO}} = \frac{r_s}{D_A(z_g)}. \quad (2.53)$$

Because of this, we can analyze the galaxy angular power spectrum at redshift z_g , to search for oscillations that indicate the BAO scale, and use this information to constrain cosmological information. A common way to do this is comparing the scale where BAO is detected to a reference scale determined with a fiducial cosmology:

$$\alpha = \frac{\theta_{\text{BAO}}^{\text{fid}}}{\theta_{\text{BAO}}} = \frac{r_s^{\text{fid}}/D_A^{\text{fid}}(z_g)}{r_s/D_A(z_g)} = \frac{r_s^{\text{fid}}D_A(z_g)}{r_sD_A^{\text{fid}}(z_g)}. \quad (2.54)$$

This comparison is quantified by a scale shift parameter known as α . If the acoustic oscillations are at the exact same scale as the one predicted by the fiducial cosmology, one should have $\alpha = 1$. The departure of α from this reference value indicates a greater inferred difference between the fiducial cosmological parameters and the probable ones given the data. On harmonic space analysis, this re-scaling of modes is usually modeled through the transformation $C_\ell \rightarrow C_{\ell/\alpha}$.

2.4.3 Non-linear damping of the acoustic signal

As one moves towards smaller scales, features of structured objects affect more and more the power spectrum. In scales where matter is predominantly collapsed into

structure, this reorganization makes it harder for the acoustic signal to be seen. Therefore, on non-linear scales, the BAO feature on the correlation function can be significantly less prominent than theory predictions. On harmonic space, this means the oscillations are damped, while on configuration space the BAO peak is broadened (BURDEN et al., 2014).

A usual way to counter this effect is through a reconstruction method, where the effects of peculiar velocities are studied and used to try to restore an original, more prominent BAO signal. Eisenstein, Seo, et al. (2007) propose a reconstruction method that restores the amplitude of the matter power spectrum oscillations to its expected value for samples of low redshift.

If we do not want to rely on reconstruction, damping can be taken into account through a combination of the original matter power spectrum with a smooth spectrum (lacking BAO signal). Such a combination relies on modeling a damping scale that tells us how fast damping arises with the progression into small scales. Template methods of this kind were used on the Dark Energy Survey Year 1 analysis, following the methodology proposed by Chan et al. (2018), and continued to be used on Year 3 analysis, with the difference that for Year 3 data the damping scale was inferred directly from the fiducial cosmological parameters, instead of being measured on mock catalogs.

THE DARK ENERGY SURVEY AND ITS BAO EFFORT

3.1 THE DARK ENERGY SURVEY

3.1.1 History

During the 2000s decade, a photometric sky survey project was proposed, with its main goal to constrain the equation of state of Dark Energy. The project involved building a camera which would be installed on the Victor Blanco Telescope, in Chile.

The proposed idea was for the camera to record images near the optical and infrared regions, so that galaxies with high redshifts could be seen clearly. An initial proposal included five years of measurements; later, the duration was extended to include a sixth year (LAHAV; CALDER; MAYERS, 2020).

The project was called the Dark Energy Survey (DES) (DES COLLABORATION; ABBOTT; ALDERING, et al., 2005), and four probes were suggested for data analysis: Galaxy clustering, Baryon Acoustic Oscillations (BAO), Type Ia supernovae and weak lensing. Each of these research lines can constrain cosmological parameters independently. A combined result could benefit from the mitigation of errors that are particular to each one of the methods.

After the camera was built, the survey was finally put to work and functioned through the 2013-2019 period. Up to now, data from the first half of this time span has already been analyzed. Its large number of results papers indicates the relevance of the survey, and how its data can be used for even more probes than the ones that were originally proposed.

3.1.2 Galaxy Clusters, supernovae and weak lensing

Galaxy cluster abundance is studied by the DES through number counts and measures of their mass and spatial distribution. These can yield information about the growth of density perturbations (DES COLLABORATION; ABBOTT; ALDERING, et al., 2005), leading to constraints on dark energy.

Weak lensing is mapped on shear catalogs, which measure distortion on the shape of source galaxies caused by the presence of lens galaxies between them and the observer (GATTI et al., 2021). From these catalogs, a tomographic analysis is performed, with a measurement of shear 2-point correlation functions. Results from shear correlation functions are often combined with galaxy-shear cross-correlation and galaxy autocorrelation results. This combination is called a 3x2pt analysis, since it combines three different 2-point functions (DES COLLABORATION; ABBOTT; ABDALLA; ALARCON; ALEKSIC, et al., 2018).

Finally, the survey also measures light curves from type Ia supernovae, in order to probe cosmology from their distance measurements, reducing uncertainties of previous measurements through careful consideration of systematic effects (COLLABORATION et al., 2019). Besides gaining precision, comparison between results from these different lines of research can help identify eventual tensions in parameter estimation, which may motivate theoretical developments in cosmology.

3.1.3 Survey camera and footprint

The camera device used by the collaboration is called the DECam, and has a field of view of 2.2 deg and five bands for photometry (*grizY*). Its specifications and the process of construction are explained in detail by Flaugher et al. (2015).

The first year of DES measurements covered an area of $1800deg^2$, and generated the Y1 GOLD catalog (DRLICA-WAGNER et al., 2018). The two posterior releases, Y3 and Y6, span $5000deg^2$. A comparison between the footprint of each catalog is shown on Figure 3.1.

3.2 THE BAO EFFORT

The possibility of using BAO as a cosmological probe on high redshift surveys has long been explored. Preliminary forecasts, such as Seo and Eisenstein (2003), paved the way for the certainty that DES would benefit of a consistent and thorough BAO measurement effort.

Usually, a three-dimensional measurement of the BAO scale can be used to estimate both the Hubble parameter and the angular diameter distance (BEUTLER et al., 2011; CUCEU et al., 2019). However, due to the characteristic reduced precision of pho-

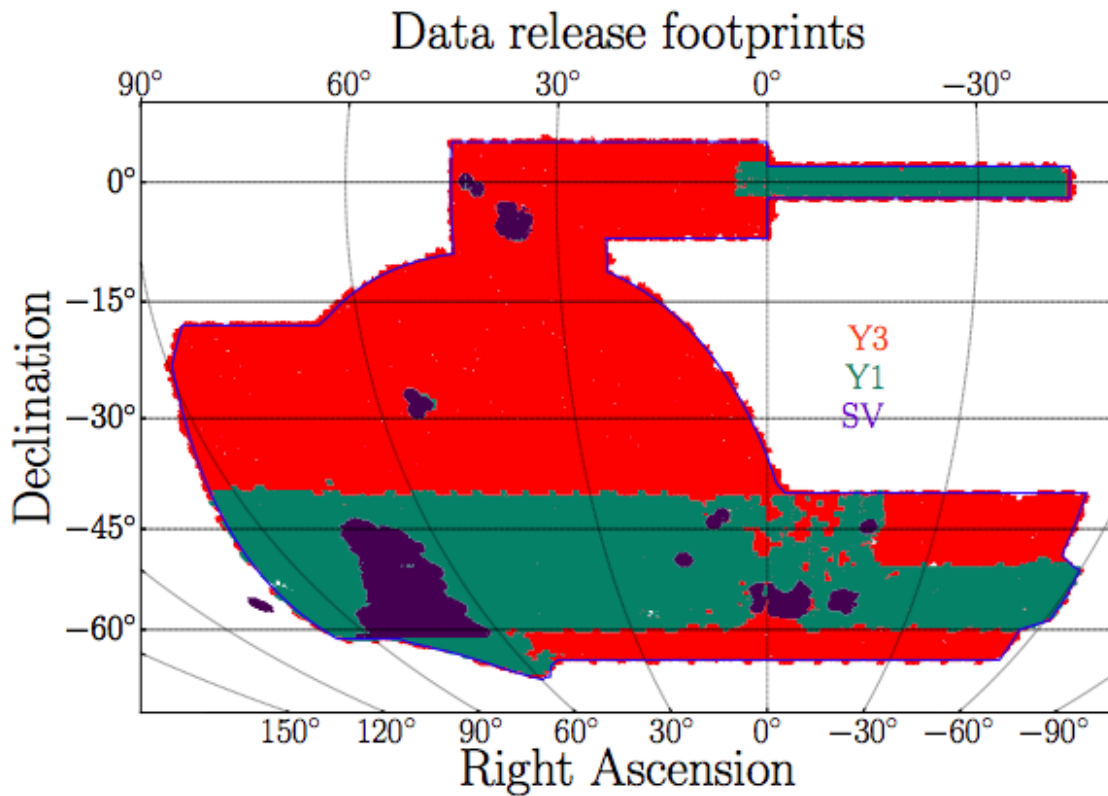


Figure 3.1 – Sky area covered by DES Y1 and Y3 catalogs. Figure from [Sevilla-Noarbe et al. \(2021\)](#)

tometric redshifts, the best use of DES data would be through a tomographic analysis. Because of this, the ability of a Hubble parameter measurement through BAO would be lost. The main DES BAO result, therefore, is the angular diameter distance as a function of the redshift ([CROCCE et al., 2018](#)).

As we saw in section 2.2, the distance itself hints into combinations of cosmological parameters. This is why the BAO measurement can contribute to the larger context of probing dark energy models.

3.2.1 Year 1 sample characterization

For the first year of data, a sample of galaxies was selected for BAO analysis following specific criteria to make the best use of the available data. [Crocce et al. \(2018\)](#) describe this selection and discuss why some choices were made by the collaboration working group.

First, they discuss the importance of selection based on precision of the redshift estimation. Even though the correlation functions are to be projected into redshift bins,

the general precision of photo- z estimation affects the errors of the projection routine. This motivated the BAO team to look at Luminous Red Galaxies (LRGs) as a possible choice for DES. An LRG sample is a subset of the Brightest cluster Galaxies (characterized by [Postman and Lauer \(1995\)](#)) where only intrinsically red galaxies are selected ([EISENSTEIN; ANNIS, et al., 2001](#)). LRGs have been often used on SDSS analyses, such that [Crocce et al. \(2018\)](#) mentions a paper where a photometric sample is constructed based on an SDSS LRG catalog ([PADMANABHAN et al., 2005](#)). The improved precision of redshift estimation is a consequence of a specific break in the spectrum of those galaxies, close to 4000\AA , that has been long studied (see [Hamilton \(1985\)](#)).

The DES collaboration did not limit itself to LRGs, but decided for a red galaxy sample, mostly populated by LRGs, that would have an optimal equilibrium between maintaining high photo- z precision without being too sparse ([CROCCE et al., 2018](#)).

3.2.2 Results from Year 1

The main BAO results from Year 1 were presented in [DES Collaboration, Abbott, Abdalla, Alarcon, Allam, et al. \(2018\)](#). This paper gathers results done with three different methodologies, each one described on a different DES methods paper: The first one uses the angular correlation function ([CHAN et al., 2018](#)); the second, a projected three-dimensional correlation function using photometric redshifts to estimate the distances ([ROSS; BANIK, et al., 2017](#)); and the third, the angular power spectrum ([CAMACHO et al., 2019](#)). The results are all consistent with each other, but the one from configuration space analysis was chosen to be the main DES Y1 result, due to its robustness during the validation process.

The authors mention how the upcoming Y3 results would probably have half the uncertainty of the Y1 results, because Y3 data includes the whole survey area of 5000 squared degrees, as opposed to the partial area covered by Y1 measurements. These new results will still be far from the precision needed to give us any insight on the important issues of cosmology; however, as the paper suggests, every DES BAO effort serves as training for upcoming work on next generation of surveys, such as the LSST ([ZHAN; TYSON, 2018](#)) (At the time, Large Synoptic Survey Telescope, later renamed Legacy Survey of Space and Time). Besides that, the Year 3 result was predicted to be one of the most precise angular diameter distance measurements ever done, which is impressive

given the fact that it would use only photometric data.

The goal of BAO analysis in DES will only be completed after all six years are analyzed—at that point, a final distance measurement will be found and compared with results from other cosmological experiments. Our contribution, however, can already be seen as the Y3 result is plotted with these other measurements. We now proceed to explain our methodology for the Y3 data analysis.

METHODS AND SIMULATIONS FOR DARK ENERGY SURVEY YEAR 3 ANALYSIS

4.1 CODE FOR THE THEORETICAL GALAXY APS

The methods used for our Y3 data analysis were almost integrally based on the methods from the Y1 harmonic space effort, described in [Camacho et al. \(2019\)](#). The first ingredient for a functional BAO detection code on harmonic space is a pipeline to generate the Angular Power Spectrum based on a specific cosmological input. This input is first used to create a three dimensional power spectrum template. Then, the projection equations are applied for a select amount of different redshift bins, the same ones by which the data is sorted.

Most DES scientists from the BAO group use the Cosmology framework ([ZUNTZ et al., 2015](#)) to construct models that perform this calculation. We developed a parallel, authorial code on python and interacted with the collaboration during the analysis in order to compare our approach with the one taken by the group.

Our code first uses the publicly available *Code for Anisotropies in the Microwave Background* ([LEWIS; CHALLINOR; LASENBY, 2000](#)), known as CAMB, to generate the matter power spectrum from input cosmological parameters. The output spectrum can be linear or non-linear, depending on the usage of specific fitting models for non-linearities. Though we only dealt with linear scales, we generated non-linear spectra selecting the halofit model ([TAKAHASHI et al., 2012](#)) on CAMB.

Following the computation of a three dimensional spectrum, the code proceeds to build a template spectrum that takes non-linear damping of the acoustic oscillations into account. First, a smooth spectrum is generated, with no BAO signal. We will call this the no-wiggle power spectrum ([VLAH et al., 2016](#)). Since its form is simple, composed of an ascending and a descending part, we used a curve optimization code to fit a second-degree polynomial to each of these parts on a logarithmic space plot of the original power spectrum. The parameters were found for the whole range of redshifts covered by the five redshift bins of the Y3 BAO analysis; thus, we were able to define a function that gives

a no-wiggle power value $P_{\text{nw}}(k, z)$ for all relevant scales and redshifts.

A combination of our simple P_{nw} model and the CAMB matter power spectrum $P(k, z)$ was then used to generate a template $P_{\text{temp}}(k, z)$. We followed the damping method from Chan et al. (2018) (see Eq. 4.1), with an updated damping scale from DES Collaboration, Abbott, Aguena, et al. (2021).

$$P_{\text{temp}}(k, z) = \left[P(k, z) - P_{\text{nw}}(k, z) e^{-k^2 \Sigma^2} \right] + P_{\text{nw}}(k, z). \quad (4.1)$$

DES Collaboration, Abbott, Aguena, et al. (2021) shows how the damping scale can be derived from the cosmology, and gives two values for it. The first one, $\Sigma = 5.8 h^{-1} \text{Mpc}$, is derived from the cosmology of mocks; and the second, $\Sigma = 5.3 h^{-1} \text{Mpc}$, from the reference cosmology of the Y3 data analysis.

With these components, the code applies the Limber approximation (Eq. 2.48) to project the power spectrum on all five redshift bins and generate one $\ell \times C_\ell$ table for each bin. The galaxy bias is assumed to be scale-independent, and its value, for each redshift bin and for all analyses performed on this project, is the one reported by DES Collaboration, Abbott, Aguena, et al. (2021) as measured value from mock catalogs (see Eq. 4.2).

$$b_g = [1.576, 1.595, 1.694, 1.821, 2.033] \quad \text{for } z\text{bin} = [1, 2, 3, 4, 5]. \quad (4.2)$$

The C_ℓ tables are then interpolated to create our final theoretical angular power spectrum functions that can be quickly called during template fitting.

4.2 SPECTRUM MEASUREMENTS

In order to compare a theoretical template spectrum with real data, one needs to be able to measure the spectrum from galaxy maps. Starting from a number count map, the angular power spectrum is defined by Eq. 2.43.

Here an issue arises, because this equation depends on a full sky measurement. Once we deal with surveys of specific regions of the sky, there needs to be a routine to extract the full sky angular power spectrum based on this partial data. P. J. E. Peebles

(1973) expresses this concern and explains how a spectrum renormalization would be needed. The idea is to recover an estimator of C_ℓ coefficients with the same statistical properties as those of full-sky spherical harmonics coefficients.

During the 1990s, various methods were explored to do this calculation, most of them based on Maximum Likelihood or quadratic estimators (HIVON et al., 2002; TEGMARK, 1997). These methods worked well for the size of data vectors used at that time, but they can become computationally expensive with the scaling of survey image size, since their operations are $\mathcal{O}(N^3)$, where N is the number of pixels (BOND; JAFFE; KNOX, 1998).

Wandelt, Hivon, and Górski (2001) presented an algorithm known as Pseudo-Cl, which deals with this problem by using analytical expressions for the likelihood of a partial sky \tilde{C}_ℓ with low computational cost. A hybrid method can also be used (EFSTATHIOU, 2004), with large scales being computed with usual MLE methods and Pseudo-Cl for small scales (large ℓ values).

The Pseudo-Cl algorithm led to the development of a method called MASTER (Monte Carlo Apodised Spherical Transform Estimator) (HIVON et al., 2002). It uses a mode coupling matrix $M_{\ell\ell'}$ that depends only on the geometry of the survey, and defines the C_ℓ estimate as on Eq. 4.3 (Eq. 15 of Hivon et al. (2002)), where $F_{\ell'}$ is a filtering function to reduce noise or features from large scale anisotropies, $B_{\ell'}$ is a window function, and \tilde{N}_ℓ the noise spectrum.

$$\langle \tilde{C}_\ell \rangle = \sum_{\ell'} M_{\ell\ell'} F_{\ell'} B_{\ell'}^2 \langle C_{\ell'} \rangle + \langle \tilde{N}_\ell \rangle. \quad (4.3)$$

For the DES analysis, measurements from mock galaxy maps and from real data were done with the NaMaster, a publicly available code designed specifically for the upcoming LSST collaboration, and described in detail in Alonso, Sanchez, and Slosar (2019).

4.3 MOCK GALAXY CATALOGS

After we have theoretical spectra and a measuring procedure, we need controlled, simulated data in order to validate our methodology. The DES collaboration, for its analysis of Year 3 data, used two sets of mock galaxy catalogs with this purpose.

4.3.1 COLA

The first mock catalog set is described by Ferrero et al. (2021), and was generated using the COLA fast n-body simulation method from Tassev, Zaldarriaga, and Eisenstein (2013). This method consists in separating large scale from small scale evolution and performing the two calculations separately.

Usual n-body simulations need a large amount of timesteps in order to retain precision. However, large scales, up to where behavior is mildly non-linear, can be dealt with theoretically, using first order Lagrangian Perturbation Theory (TASSEV; ZALDARRIAGA, 2012). Performing n-body evolution only at small scale while updating large scale with exact theoretical values allows for a detailed output with an order-of-magnitude reduction on the number of timesteps (TASSEV; ZALDARRIAGA; EISENSTEIN, 2013).

The specific routine used to generate these mocks, with the optimal parameters to balance computational speed and accuracy on the relevant scales, was developed by Izard, Crocce, and Fosalba (2016), and it is known as ICE-COLA. A set of 488 light-cone simulations was used, each simulation supplying a total of 4 catalogs after the DES footprint mask is applied. This gives a total of 1952 mock measured spectra. All mocks were generated with the same cosmology as the MICE *Grand Challenge* n-body simulation (FOSALBA et al., 2015), and tests were performed to compare up to which scale the fast simulations match the full N-body results.

After the final dark matter halo catalog was generated, the next step was to produce a galaxy catalog matching the characteristics of the DES Y3 BAO sample. This was done with the hybrid HAM-HOD method from (AVILA et al., 2018), and the adaptation of Avila et al. (2018)'s routine to the Y3 scenario is described in detail by Ferrero et al. (2021).

4.3.2 FLASK

A second set of mock catalogs was generated by the collaboration with a lognormal distribution method, that avoids having to evolve an n-body simulation from an early redshift. Instead, it simulates directly the current galaxy distribution map, divided in tomographic bins. A total of 2000 catalogs was built with the FLASK code (XAVIER; ABDALLA; JOACHIMI, 2016), with input correlation functions and galaxy bias values extracted from the set of COLA mocks (see Eq. 4.2).

4.4 COVARIANCE

The covariance of the galaxy APS can be estimated through purely theoretical calculations or it can also be measured from mock catalogs. Theoretical covariances are often based on a separate modeling of the Gaussian and the non-Gaussian terms, and [DES Collaboration, Abbott, Aguena, et al. \(2021\)](#) conclude that there is little difference when the non-Gaussian terms are added, which makes their consideration unnecessary of the intended analysis.

For our project, we used the baseline theoretical covariance produced by the BAO working group at DES for their Y3 analysis. This covariance was modeled according to [Garcia-Garcia, Alonso, and Bellini \(2019\)](#), who use pseudo- C_ℓ estimators to account for terms from mixed harmonic modes that arise when the spectrum is measured from partial-sky maps. An initial diagonal approximation would look like Eq. 4.4 (Eq. 19 from [DES Collaboration, Abbott, Aguena, et al. \(2021\)](#))—where f_{sky} is the fraction of the sky covered by the survey and n_g the galaxy number density), to which the effect of masking is then added.

$$\text{Cov}(C_\ell, C_{\ell'}) = \frac{2\delta_{\ell\ell'}}{f_{sky}(2\ell + 1)} \left(C_{\ell'} + \frac{1}{n_g} \right)^2. \quad (4.4)$$

The code used by DES to perform these calculations is called *CosmoLike*, and was presented by [Krause and Eifler \(2017\)](#). After a full covariance matrix was obtained, it was validated with measurements from both mock catalogs. Sufficient agreement was achieved with the FLASKs, but a discrepancy in the covariance between different redshift bins arose for COLA. This is due to the fact that each COLA lightcone is used to produce 4 mocks, so it is a limitation of the simulation method itself ([FERRERO et al., 2021](#)).

4.5 STATISTICS FOR TEMPLATE FITTING

Having our theory, data vectors and covariance, we take a brief look at the statistical methods used to constrain theoretical parameters. Two different approaches are used for this kind of analysis¹.

¹ A comparative presentation of both approaches can be found in [Wakefield \(2013\)](#).

4.5.1 Frequentist statistics

The classical approach to statistics, also known as the frequentist approach, is based on an objective definition of probability. Given an experimental setting, probability is defined as the limit of the ratio between occurrences of an event and the total number of trials when the latter tends to infinity (BARLOW, 2013). In this sense, it is related to frequency, and may be ill-defined when we do not have a reproducible experiment in mind.

The most well known frequentist method for parameter fitting is the Maximum Likelihood Estimator (MLE). A likelihood function is defined to be proportional to the combined probability of each data point relative to a specific model. Therefore, it is a function of the model parameters p . Usually, we assume the points to be drawn from Gaussian distributions whose width is given by their estimated uncertainty. In this case, the likelihood is given by Eq. 4.5.

$$\mathcal{L}(p) \propto e^{-\chi^2(p)/2}, \quad (4.5)$$

where

$$\chi^2(p) = \sum_{i=0}^N \frac{(y_i - m(p, x_i))^2}{\sigma_i^2} \quad (4.6)$$

for a model function m . When different data points may be correlated, the χ^2 is obtained through the covariance matrix, as in Eq. 4.7

$$\chi^2(p) = (y - m(p))\text{Cov}^{-1}(y - m(p))^T \quad (4.7)$$

where y is the data vector and Cov the covariance matrix.

The MLE method searches for the maximum of the likelihood function, in order to get the optimal set of parameters.

4.5.2 Bayesian statistics

Following Bayes' theorem, an alternative approach to statistics can be developed, which allows prior information to be taken into account when computing probabilities. The Bayes theorem relates the probability of event A given event B to the probability of B given A (Eq. 4.8).

$$P(A|B) = \frac{P(B|A)P(A)}{P(B)}. \quad (4.8)$$

The goal of bayesian methods is to estimate the posterior probability distribution of the parameters p given the observed data D . From the theorem, this probability is

$$P(p|D) = \frac{\mathcal{L}(p)P(p)}{P(D)} \quad (4.9)$$

where $P(p)$ is an a priori probability distribution known as *prior*.

A common method to sample this posterior is the Monte Carlo Markov Chain (MCMC). It works by drawing random samples following a chain where the probability of a drawing depends only on the previous sample (BROOKS, 2011). MCMC sampling, when compared with maximum likelihood estimation, has the advantage that it yields the whole distribution as a result, instead of a single optimal value and its uncertainties. Thus, any degeneracy between different parameters is more easily spotted.

When interpreting results from statistical bayesian inference, we need to be careful not attribute more meaning to a result than it actually has. Even though Bayes's theorem provides a logical framework, all measures of evidence are relative, and models can only be assessed as more probable in comparison with other existent models (MASSIMI, 2021). In this sense, there is no fundamental epistemological difference between results from frequentist or bayesian techniques. The difference lies more in the broadness of the method—bayesian analysis can include classical methods while also incorporating more prior knowledge into the statistical sampling.

4.6 FINAL MODEL

The final BAO model should account for the presence of non-linear effects at small scales, as well as for re-scaling of the whole spectra, once the input galaxy bias values are only tentative. A basic model, with a single term for small scale features, would look like Eq. 4.10

$$C_\ell^{\text{model}} = BC_{\ell/\alpha} + A. \quad (4.10)$$

Each redshift bin would be modeled this way, with its own B and A parameters. The scale parameter, however, is a global measurement, so it is the same for all bins.

Since the Y1 analysis discussions, the collaboration has come to understand that more terms are needed to model unknown small scale features. The current model used

for the main Y3 result (Eq. 4.11) includes 4 broadband terms, giving a total of 5 terms per redshift bin plus the scale parameter.

$$C_{\ell}^{\text{model}} = BC_{\ell/\alpha} + \sum_{i=-1}^3 A_i \ell^i. \quad (4.11)$$

DES Collaboration, Abbott, Aguena, et al. (2021) show a comparison between BAO fits with this model and previous versions of it, with $i = 0$; $i = 0, 1$; $i = 0, 1, 2$. The full model is shown to move the $\langle \chi^2 \rangle / dof$ slightly towards 1, and is therefore selected as the baseline choice.

RESULTS

Our results chapter is divided as follows. First, we deal with the work done with the set of FLASK simulations. This includes the optimization of measurements with the Pseudo-Cl method and some preliminary BAO fits. Then, we move to the COLA simulations, exploring the BAO scale measurements with both Maximum Likelihood Estimators and Monte Carlo chains. Finally, we show our independent measurements for Y3 data together with the main collaboration result, and we use the obtained parameter to compute the angular diameter distance at redshift $z_{\text{eff}} = 0.835$. On Appendix A, we report our progress on a side project that applies the same methodology from our harmonic space analysis to constrain primordial non-Gaussianities on the angular power spectrum.

5.1 FLASK MOCK MEASUREMENTS AND PRELIMINARY TESTS

These tests were performed during the first stage of our project, during 2019, while the Dark Energy Survey collaboration was performing measurements on the mentioned set of FLASK mocks.

5.1.1 The effect of $\Delta\ell$

We started with a single simulation and measured the Angular Power Spectrum of the first redshift bin with three different linear binning schemes. The obtained data points are compared with our theoretical spectrum on Figure 5.1. As expected, there is less statistical noise on the measured curve for higher values of $\Delta\ell$, at the cost that any real oscillatory feature could be less distinguishable.

We then tested how linear binning schemes would affect the χ^2 per degrees of freedom for a simple fit with a scaling factor as the only parameter, for a combination of three different scale cuts on large scales and two different scale cuts on small scales. Results are shown on Figure 5.2, and we did not identify any relevant trend that would require attention when deciding binning schemes and scale cuts for the collaboration.

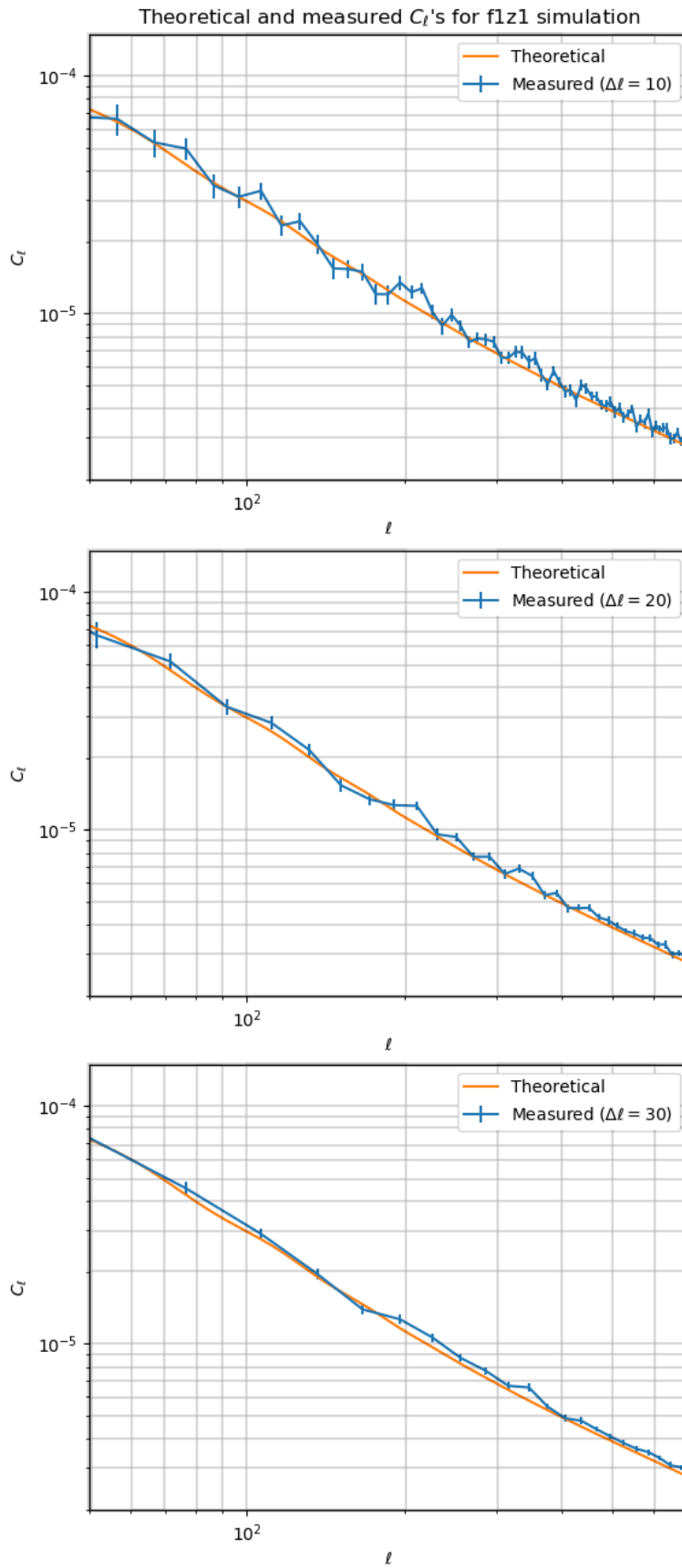
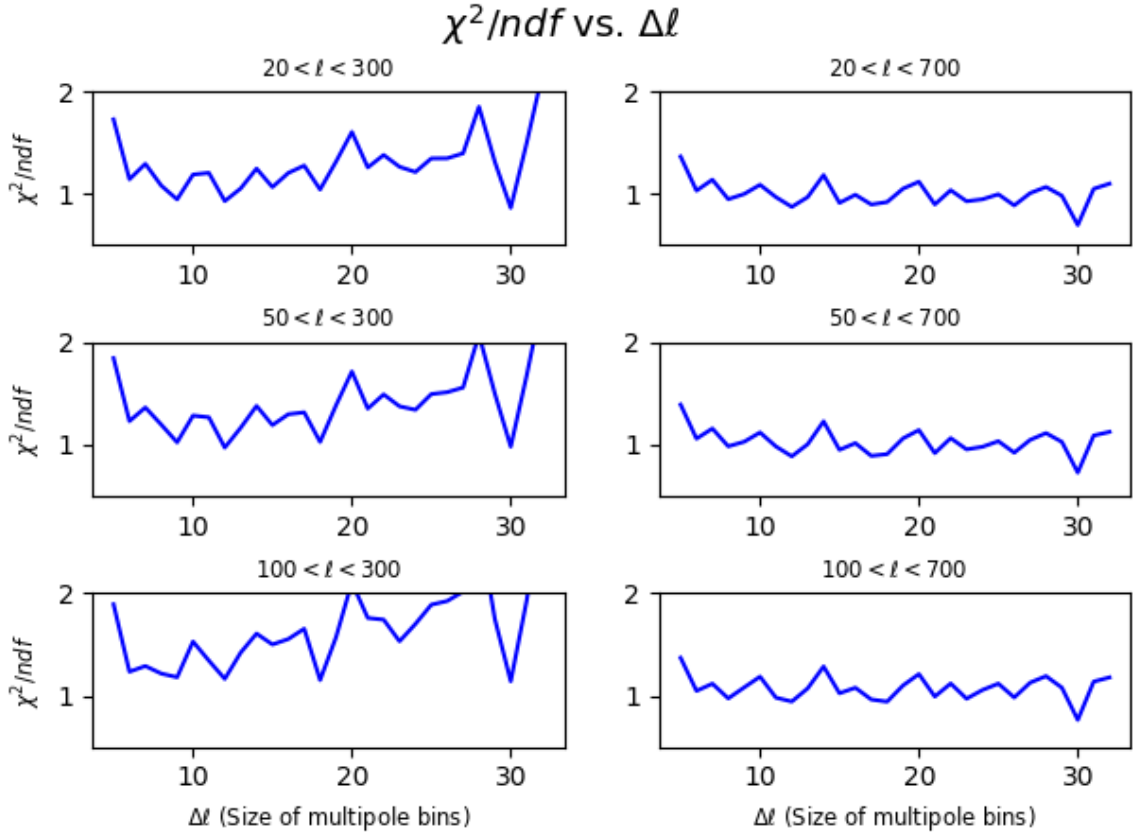


Figure 5.1 – Comparison between theoretical and measured C_ℓ 's from a single map (identified as flz1) with $\Delta\ell = 10, 20, 30$.

Figure 5.2 – χ^2 as a function of the size of multipole bins.

<i>Model</i>	α	χ^2/ndf
Template	1.009 ± 0.036	1.776
No-wiggle	1.09 ± 0.33	2.62

Table 5.1 – Best fit parameters for two models. Uncertainty values were extracted directly from the covariance matrix given by the optimization code output.

5.1.2 BAO measurement with MLE

We used the first 50 FLASK mocks and the first redshift bin in order to perform a first BAO measurement, as a way of testing our methodology and codes. We used $\ell \in [50, 300]$, a sample region containing most of the BAO feature. Two optimization runs were performed: one with the template spectrum from Eq. 4.11 and the other with a no-wiggle spectrum (a projection of the no-wiggle $P(k)$ from Section 4.1). Results for the scale parameter α are shown on Table 5.1. The error of the parameter from the no-wiggle fit was found to be one order of magnitude greater than the error when using the template. This is clear evidence of how the parameter measures the location of a specific feature that is present in the first model and not present in the second one.

5.2 COLA MOCK MEASUREMENTS

For the set of 1952 COLA mocks, we performed all calculations with the template from Eq. 4.11. The APS data points were measured from the galaxy catalogs with bins of $\Delta\ell = 20$, starting from $\ell_{min} = 10$ up to the scale where the spectrum starts deviating from linear regime. This scale was determined by the collaboration to be around $k_{max} = 0.25hMpc^{-1}$ (DES COLLABORATION; ABBOTT; AGUENA, et al., 2021). The scale cuts on harmonic space were determined following the Limber approximation relation (Eq. 2.49) at the distance of the mean redshift of each z -bin. This resulted in $\ell_{max} = [410, 470, 510, 550, 610]$ for $zbin = [1, 2, 3, 4, 5]$.

We used our Maximum Likelihood Estimator to obtain a value of α for the mean of all 1952 mocks, as well as one for each individual mock. For the individual mocks, we first took the average and standard deviation of α values; then, we performed the sum of all individual probability density functions and extracted a mean value and sigma from a gaussian fit. The average χ^2 per ndf was $\chi^2 = 99.2/104$.

As a form of validation, the measurement on the mean of mocks was repeated with MCMC sampling. We used the python Ensemble Sampler *emcee* (FOREMAN-MACKEY et al., 2013) with an initial state of $\alpha = 1$ and, for all redshift bins, $B = 1$, $A_i = 0$ for $i \in (-1, 0, 1, 2)$. The scaling factors B were bounded to be positive.

Our MLE results are shown on Table 5.2, where they are also compared with the equivalent number from independent analysis by the BAO working group at the DES Collaboration (DES COLLABORATION; ABBOTT; AGUENA, et al., 2021). Figures 5.3 and 5.4 show the distribution of the obtained α values from individual mocks, the former with a gaussian fit for the single-value distribution and the latter with a fit for the sum of all PDFs. Figure 5.5 shows the corner plot for our MCMC sample. We show only the scaling factor and ignore the other nuisance parameters for convenience.

These results show that the expected $\alpha = 1$ cosmology is successfully extracted from the mocks. Since the simulations were made with specific cosmological parameters as their input, and the theory APS has the same parameter values, deviations from α would probably indicate an error in our pipeline. Fortunately, that was not the case.

The order of magnitude of the uncertainties are all the same, and they indicate the precision level we were expected to achieve with the Y3 data analysis.

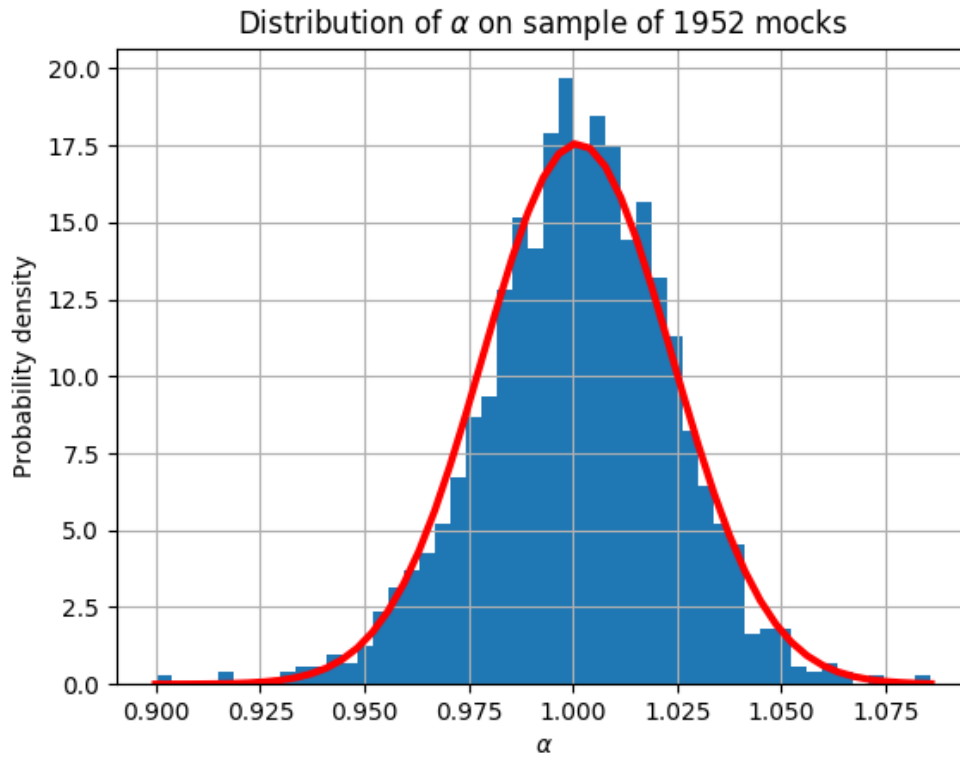


Figure 5.3 – Distribution of BAO scale parameter α on the full set of COLA mocks: Histogram with simple gaussian fit.

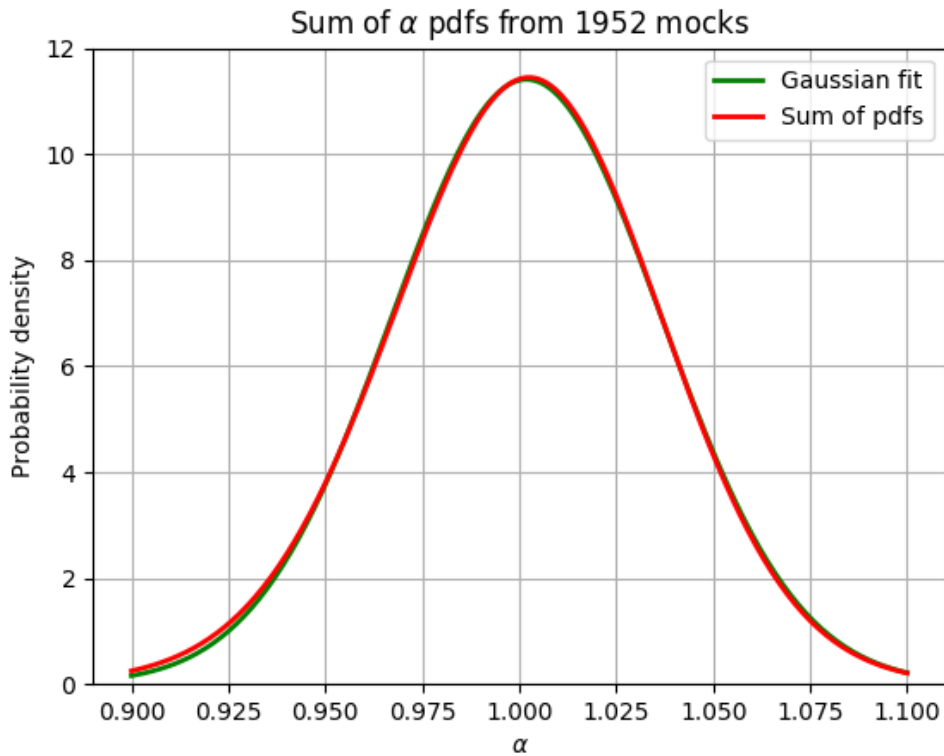


Figure 5.4 – Distribution of BAO scale parameter α on the full set of COLA mocks: Sum of individual probability density functions and a gaussian fit of the sum.

	α
Mean of mocks	1.002 ± 0.027
Average and st. dev. (1952 mocks)	1.001 ± 0.023
Gaussian fit (1952 mocks)	1.002 ± 0.035
DES Collaboration result	1.004 ± 0.023

Table 5.2 – Best fit parameters for individual and mean data vectors.

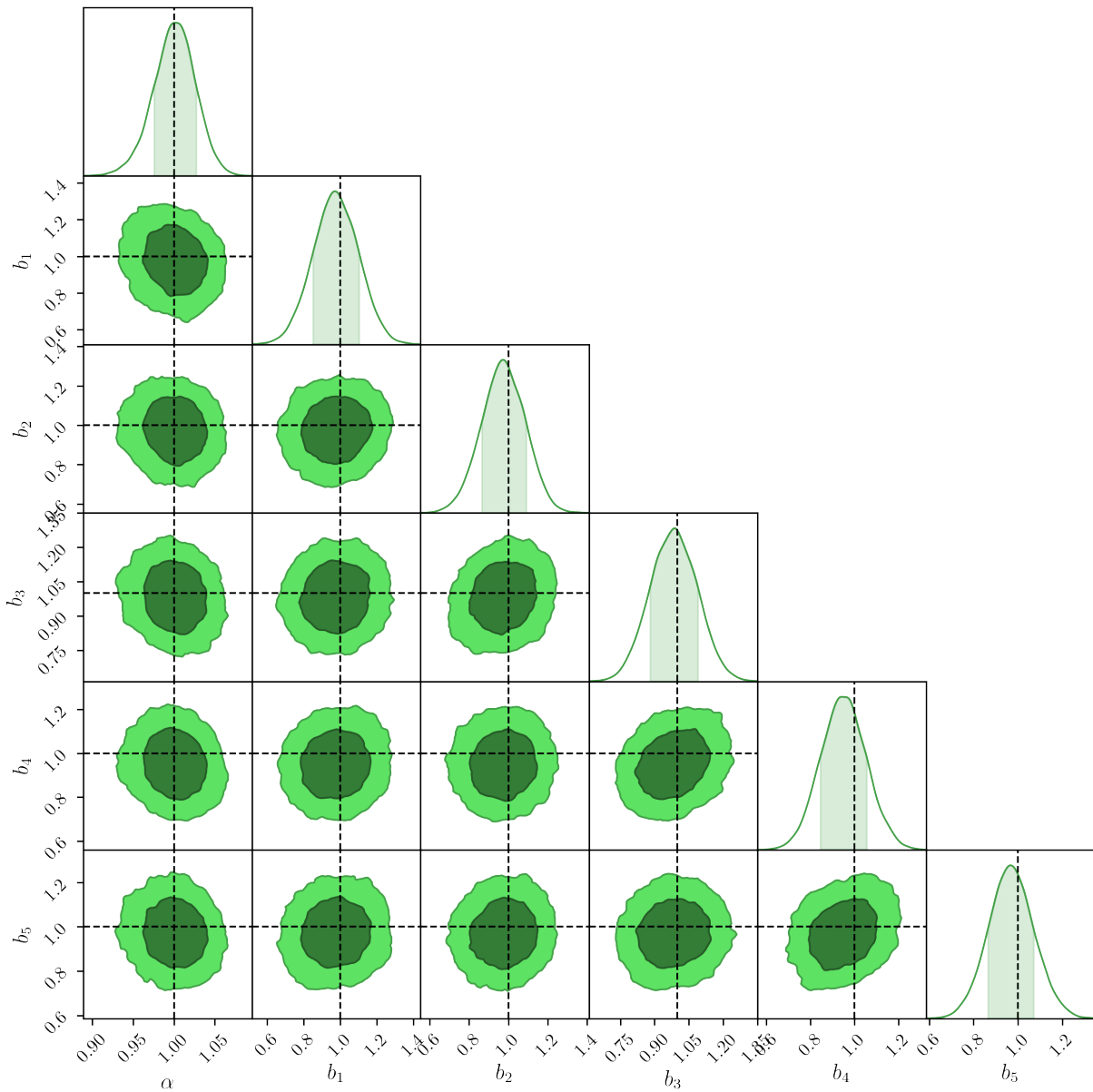


Figure 5.5 – BAO scale parameter and scaling factors for MCMC analysis of the mean of COLA mocks.

<i>Method</i>	α
MLE	0.950 ± 0.031
MCMC	$0.961^{+0.029}_{-0.028}$
DES Collaboration/MLE	0.942 ± 0.026

Table 5.3 – BAO scale parameter measured on Y3 data: Best fit for different pipelines.

5.3 Y3 DATA ANALYSIS

5.3.1 Global fits

We fed the angular power spectrum measurements from the Y3 BAO sample into our MLE and MCMC pipelines in order to perform a final BAO scale measurement. The same bounds and initial guess reported for the mock runs were used. Following a decision by the Collaboration, we used the cosmology of [Planck Collaboration et al. \(2020\)](#) as our baseline theory. Therefore, the parameter α denotes the deviation of the BAO scale in respect to this specific cosmology.

The obtained parameter is shown on Table 5.3, and the distribution of α and of the scaling factors on the MCMC chain is shown on Figure 5.6. The full set of 26 parameters with their respective errors, for both methods, is shown on Appendix B.

Constrained scaling factors do not have a physical meaning. They are supposed to indicate the difference between the real galaxy bias and our input values. However, since the vertical shift in the spectrum is also dependent on cosmological parameters, it is hard to establish any direct implication of measured values. In this sense, they work as nuisance parameters, just like the broadband terms A_i .

5.3.2 Redshift dependent fits

We then performed an analysis of each redshift bin, in order to see how they contribute to the total measurement of the scale parameter. The same template model was used, with the only difference being that the input data vector now included a single redshift bin. The obtained scale parameters are shown on Table 5.4, together with the equivalent collaboration result ([DES COLLABORATION; ABBOTT; AGUENA, et al., 2021](#)). Figure 5.8 contains parameter distributions for the 5 MCMC chains.

Both sets of MLE measurements include no detection at the first redshift bin (the error at this bin was comparable to the one obtained with a no-wiggle spectrum—this means the BAO wiggles are not actually being measured), three similar values for the

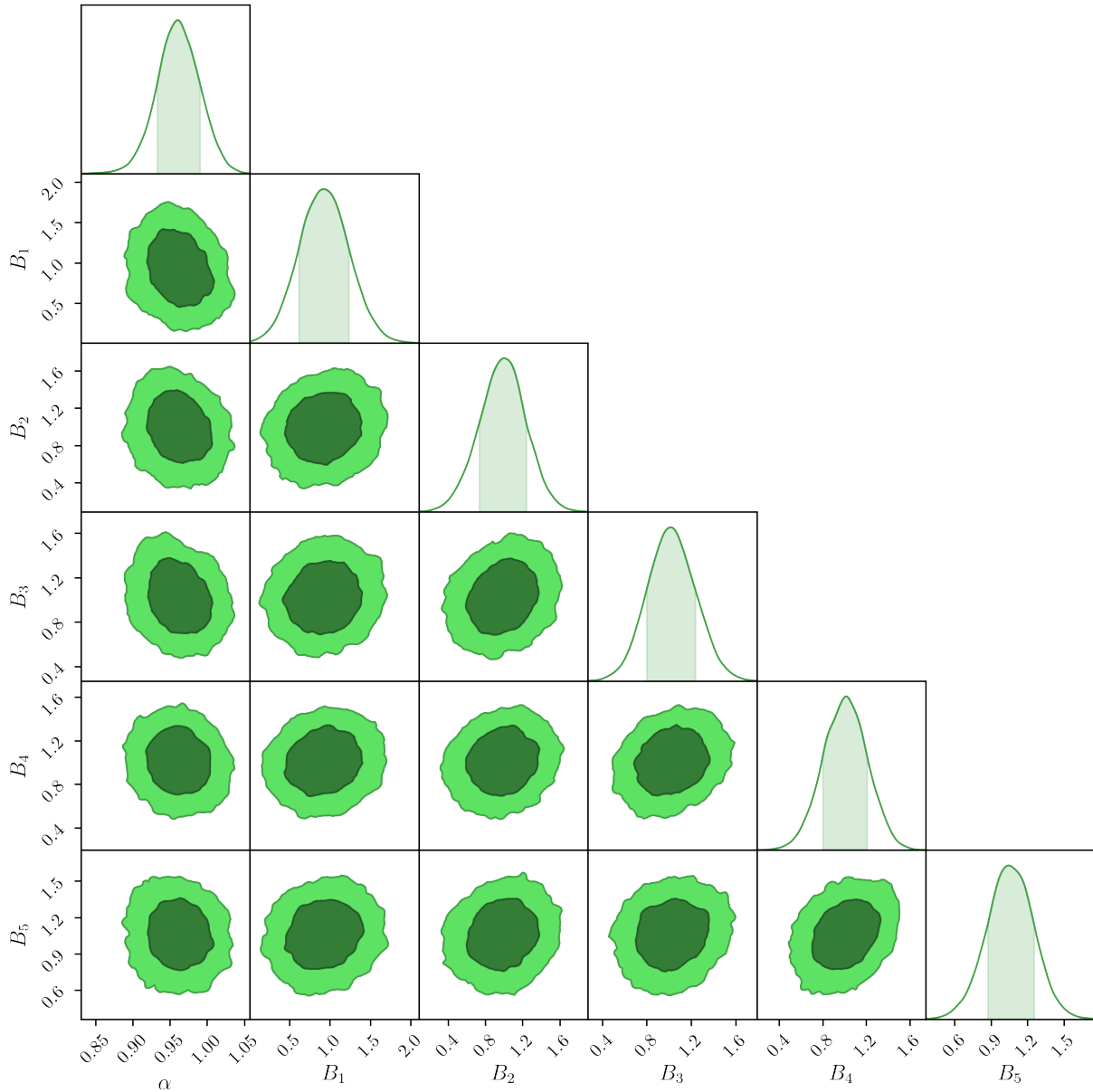


Figure 5.6 – BAO scale parameter and scaling factors for MCMC analysis of Y3 data.

intermediary bins, and a considerably smaller value for the last redshift bin (high redshifts). It can be inferred that high redshift data shifted the final BAO scale measurement apart from the baseline Planck cosmology. This can either be an expected variation between measurements or the consequence of loss of precision of the photometric redshift estimators for samples of high redshift.

We notice that this trend from the last redshift bin does not appear in our MCMC chain— α values seem much similar to each other. However, this result for redshift dependent fits is not as reliable as the MLE one. The chain distribution shows a small degeneracy between α and the scaling parameter, which makes specific features from an individual redshift bin harder to grasp. This degeneracy is due to the fact that a horizon-

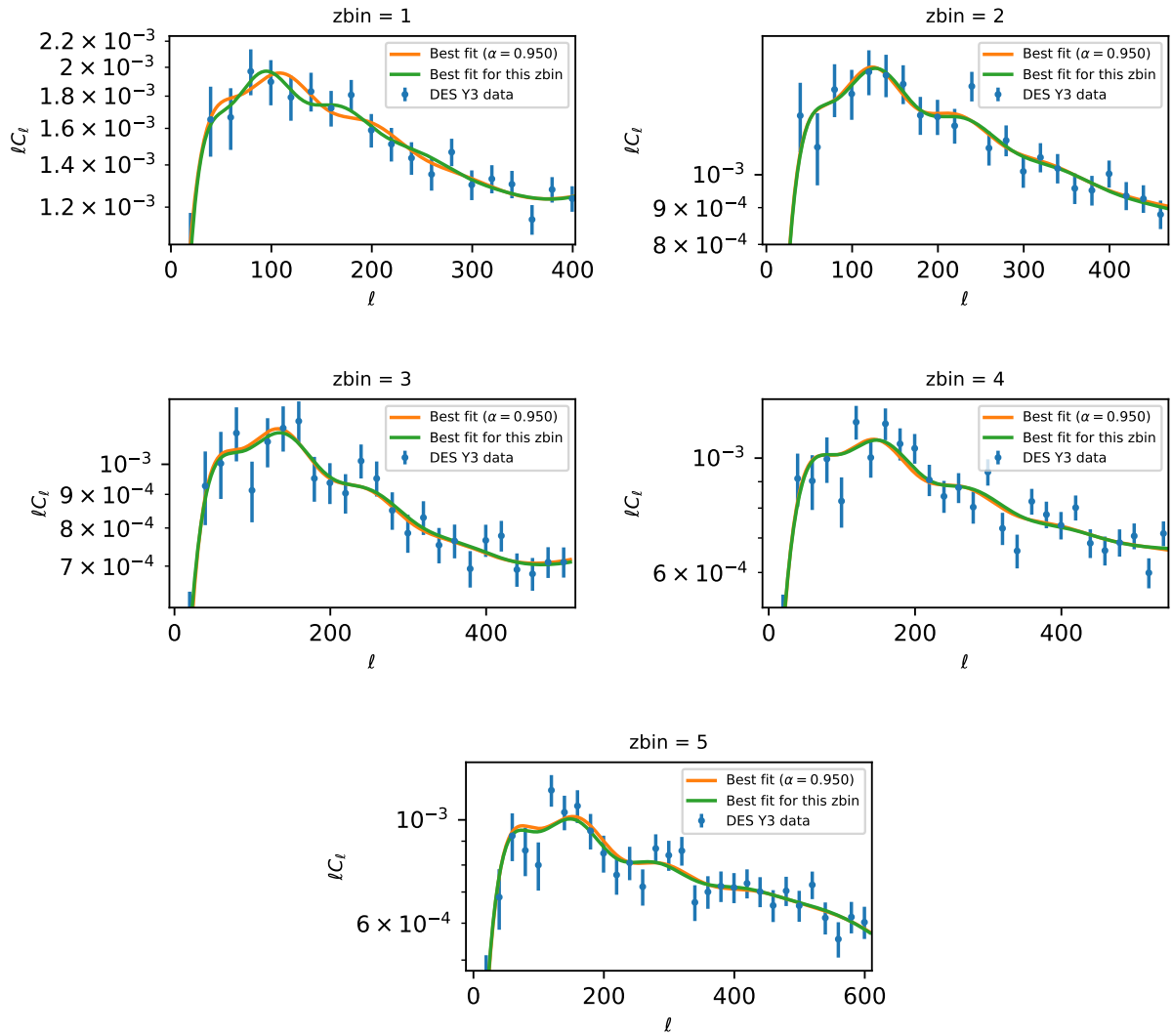


Figure 5.7 – DES Y3 measured and best fit angular power spectra.

tal re-scaling of APS modes can also produce a vertical shift. This effect is only removed when a single α is measured from the whole set of five redshift bins. Our redshift dependent fits, in this sense, cannot be taken as having a significant interpretation, apart from their helping us test the robustness of the global value.

Finally, the uncertainty values of our redshift dependent fits are systematically higher than those obtained by the collaboration, which can be a difference in the specific fitting procedure for this section of the project. A more thorough comparison with the Collaboration pipelines would be needed to identify the origin of this discrepancy.

Figure 5.7 shows the Y3 data vector together with the MLE best fit angular power spectrum for both the full calculation and the redshift dependent one.

z-bin	α		
	MLE	MCMC	DES Collaboration/MLE
1	No detection	No detection	No detection
2	0.982 ± 0.074	$0.951^{+0.085}_{-0.099}$	0.992 ± 0.055
3	0.969 ± 0.092	$0.952^{+0.082}_{-0.096}$	0.979 ± 0.053
4	0.984 ± 0.074	$0.959^{+0.072}_{-0.082}$	0.971 ± 0.038
5	0.917 ± 0.071	$0.961^{+0.077}_{-0.090}$	0.919 ± 0.040

Table 5.4 – BAO scale parameter for each redshift bin.

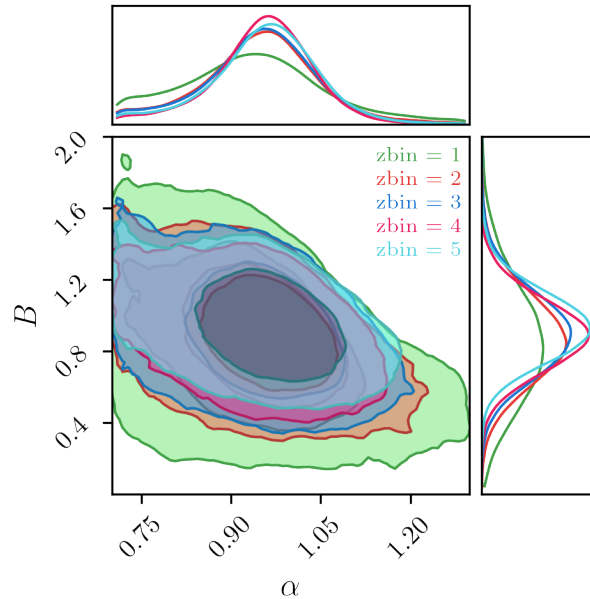


Figure 5.8 – MCMC parameter distribution for redshift dependent analysis of Y3 data.

5.4 ANGULAR DIAMETER DISTANCE

The measured scale parameter α can be put on Eq. 2.54 to find the angular diameter distance of a specific redshift in terms of the sound horizon at drag epoch. The Planck angular diameter distance ratio at the effective redshift of the Y3 BAO sample ($z_{\text{eff}} = 0.835$) is equal to $D_A(0.835)/r_s = 10.9$ (DES COLLABORATION; ABBOTT; AGUENA, et al., 2021)¹. Multiplying this value by $\alpha = 0.950 \pm 0.031$ (see Table 5.3), we get an angular diameter distance of $D_A(0.835)/r_s = 10.36 \pm 0.34$.

The relative error of this independent result is 3.3%, slightly larger than the 2.7% value obtained by the DES Collaboration. In the larger context of all sky survey projects, the DES BAO measurement has the smallest fractional error ever obtained from photometric surveys (DES COLLABORATION; ABBOTT; AGUENA, et al., 2021). Spectroscopic data, however, still yields comparable to lower uncertainties. Figure 5.9 shows the DES

¹ We divide the reported value by $1 + z$ to convert from comoving distance $D_M(z)$ to $D_A(z)$.

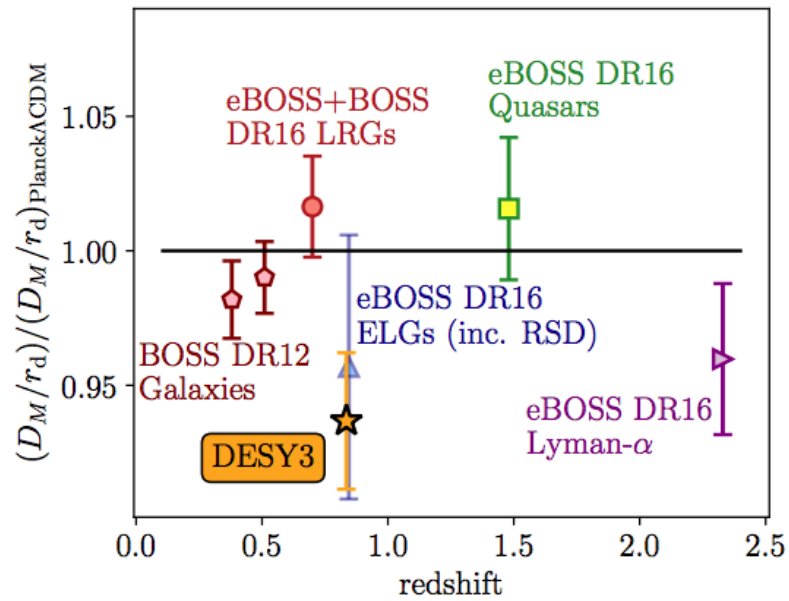


Figure 5.9 – Re-scaled angular diameter distance measurements from recent surveys. Figure from [DES Collaboration, Abbott, Aguena, et al. \(2021\)](#).

angular diameter distance (divided by the Planck value) compared to measurements from other surveys.

We can see the DES Y3 data point as the lowest in the Figure—this is a direct consequence of the fifth redshift bin pulling down the global scale measurement. Nevertheless, many tests were performed to check the robustness of the fit over uncertainties on photo- z estimation for this bin and over other possible systematic effects, and no significant changes were detected when these possibilities were taken into account ([DES COLLABORATION; ABBOTT; AGUENA, et al., 2021](#)).

FINAL REMARKS

We studied the theoretical framework of modern cosmology and how its predictions in terms of large scale clustering of galaxies are detectable by modern sky surveys. We focused on the Dark Energy Survey and its effort to detect the Baryon Acoustic Oscillation (BAO) feature from harmonic space power spectra. Following the DES methodology from Year 1, and incorporating the new simulations used for Year 3 analysis, we performed an independent validation of the Year 3 BAO measurement on harmonic space.

This validation involved the development of a code to compute theoretical angular power spectra, and for template fitting with both maximum likelihood and Monte Carlo methods. We performed tests on two sets of mock galaxy catalogs produced by the DES Collaboration: one made from lightcone fast n-body simulations, and another generated with lognormal distribution maps. These tests recovered the expected BAO scale from the cosmology of the mocks.

Results from DES data were compared with those picked as the baseline results by [DES Collaboration, Abbott, Aguena, et al. \(2021\)](#). While the collaboration presented a scale of $\alpha = 0.942 \pm 0.026$ (relative to the Planck fiducial cosmology), we achieved the value of $\alpha = 0.950 \pm 0.031$ with MLE. Both values are compatible, and this result provides an important data point on the figure of distance measurements from angular clustering.

Our contribution to the DES project got us involved in two papers of Year 3 results: the main BAO results paper ([DES COLLABORATION; ABBOTT; AGUENA, et al., 2021](#)) and the galaxy mocks for BAO paper ([FERRERO et al., 2021](#)). Together with our work with primordial non-Gaussianities (Appendix A), it provided us with experience in computational analysis for large surveys, which will be much needed for LSST.

As we hinted in Chapter 1, modern day precision cosmology is reliant on the Λ CDM model, but lacks a proper interpretation for dark energy. We hope that future constraints on BAO can be combined with these DES results in order to move cosmological parameter determination one step closer to a level where dark energy models can be actually checked against each other.

REFERENCES

- ALAM, Shadab et al. Completed SDSS-IV extended Baryon Oscillation Spectroscopic Survey: Cosmological implications from two decades of spectroscopic surveys at the Apache Point Observatory., v. 103, n. 8, 083533, p. 083533, Apr. 2021. Cited 2 times on pages 19, 20.
- ALBRECHT, Andreas et al. Report of the Dark Energy Task Force. **arXiv:astro-ph/0609591**, Sept. 2006. Cited 1 time on page 20.
- ALONSO, David; SANCHEZ, Javier; SLOSAR, Anže. A unified pseudo- C_ℓ framework. **Monthly Notices of the Royal Astronomical Society**, Oxford University Press (OUP), v. 484, n. 3, p. 4127–4151, Jan. 2019. ISSN 1365-2966. Cited 1 time on page 53.
- ALVAREZ, Marcelo et al. **Testing Inflation with Large Scale Structure: Connecting Hopes with Reality**. [S.l.: s.n.], 2014. arXiv: [1412.4671](https://arxiv.org/abs/1412.4671) [[astro-ph.CO](https://arxiv.org/abs/1412.4671)]. Cited 1 time on page 85.
- AVILA, S et al. Dark Energy Survey Year-1 results: galaxy mock catalogues for BAO. **Monthly Notices of the Royal Astronomical Society**, v. 479, n. 1, p. 94–110, May 2018. ISSN 0035-8711. Cited 2 times on page 54.
- BAHCALL, Neta A. Hubble’s Law and the expanding universe. **Proceedings of the National Academy of Sciences**, National Academy of Sciences, v. 112, n. 11, p. 3173–3175, 2015. ISSN 0027-8424. Cited 1 time on page 24.
- BARLOW, R. J. **Statistics: a Guide to the Use of Statistical Methods in the Physical Sciences**. Hoboken: Wiley, 2013. Cited 1 time on page 56.
- BARREIRA, Alexandre. IOP Publishing, v. 2020, n. 12, p. 031–031, Dec. 2020. DOI: [10.1088/1475-7516/2020/12/031](https://doi.org/10.1088/1475-7516/2020/12/031). Cited 1 time on page 85.
- BEUTLER, Florian et al. The 6dF Galaxy Survey: baryon acoustic oscillations and the local Hubble constant., v. 416, n. 4, p. 3017–3032, Oct. 2011. Cited 1 time on page 46.
- BOND, J. R.; JAFFE, A. H.; KNOX, L. Estimating the power spectrum of the cosmic microwave background. **Physical Review D**, American Physical Society (APS), v. 57, n. 4, p. 2117–2137, Feb. 1998. ISSN 1089-4918. Cited 1 time on page 53.
- BOSCH, Frank van den. **Theory of Galaxy Formation - Lecture 12: Large Scale Structure**. [S.l.]: Yale University, 2020. Available from: http://www.astro.yale.edu/vdbosch/astro610_lecture12.pdf>. Cited 1 time on page 39.

- BROOKS, Steve. **Handbook of Markov chain Monte Carlo**. Boca Raton London: CRC Press, 2011. Cited 1 time on page 57.
- BURDEN, A. et al. Efficient reconstruction of linear baryon acoustic oscillations in galaxy surveys. **Monthly Notices of the Royal Astronomical Society**, v. 445, n. 3, p. 3152–3168, Oct. 2014. ISSN 0035-8711. Cited 1 time on page 43.
- CAMACHO, H et al. Dark Energy Survey Year 1 results: measurement of the galaxy angular power spectrum. **Monthly Notices of the Royal Astronomical Society**, Oxford University Press (OUP), v. 487, n. 3, p. 3870–3883, June 2019. Cited 4 times on pages 39, 40, 48, 51.
- CHAN, K C et al. BAO from angular clustering: optimization and mitigation of theoretical systematics. **Monthly Notices of the Royal Astronomical Society**, v. 480, n. 3, p. 3031–3051, July 2018. ISSN 0035-8711. Cited 3 times on pages 43, 48, 52.
- CHAVEZ, H. O. C. **Estruturas em Larga Escala e o Dark Energy Survey**. 2014. MA thesis – Instituto de Física - Universidade de São Paulo, São Paulo. Cited 1 time on page 40.
- COLLABORATION, DES et al. First Cosmology Results using Type Ia Supernovae from the Dark Energy Survey: Constraints on Cosmological Parameters. *American Astronomical Society*, v. 872, n. 2, p. 130, Feb. 2019. Cited 1 time on page 46.
- COLLISTER, Adrian A.; LAHAV, Ofer. ANNz: Estimating Photometric Redshifts Using Artificial Neural Networks. **Publications of the Astronomical Society of the Pacific**, IOP Publishing, v. 116, n. 818, p. 345–351, Apr. 2004. Cited 1 time on page 28.
- CONLEY, A. et al. Measurement of Ω_m , Ω_Λ from a Blind Analysis of Type Ia Supernovae with CMAGIC: Using Color Information to Verify the Acceleration of the Universe. *American Astronomical Society*, v. 644, n. 1, p. 1–20, June 2006. Cited 1 time on page 30.
- CROCCE, M et al. Dark Energy Survey year 1 results: galaxy sample for BAO measurement. **Monthly Notices of the Royal Astronomical Society**, v. 482, n. 2, p. 2807–2822, Sept. 2018. ISSN 0035-8711. Cited 4 times on pages 47, 48.
- CROFT, Rupert A. C.; DAILEY, Matthew. On the measurement of cosmological parameters. **Quarterly Physics Review**, n. 1, p. 1–14, 2015. Cited 1 time on page 30.
- CUCEU, Andrei et al. Baryon Acoustic Oscillations and the Hubble constant: past, present and future. IOP Publishing, v. 2019, n. 10, p. 044–044, Oct. 2019. DOI: [10.1088/1475-7516/2019/10/044](https://doi.org/10.1088/1475-7516/2019/10/044). Available from: [<https://doi.org/10.1088/1475-7516/2019/10/044>](https://doi.org/10.1088/1475-7516/2019/10/044). Cited 1 time on page 46.

- DAWSON, Kyle S.; KNEIB, Jean-Paul, et al. The SDSS-IV Extended Baryon Oscillation Spectroscopic Survey: Overview and Early Data., v. 151, n. 2, 44, p. 44, Feb. 2016. Cited 1 time on page [19](#).
- DAWSON, Kyle S.; SCHLEGEL, David J., et al. The Baryon Oscillation Spectroscopic Survey of SDSS-III., v. 145, n. 1, 10, p. 10, Jan. 2013. Cited 1 time on page [19](#).
- DE MATTIA, Arnaud; RUHLMANN-KLEIDER, Vanina. Integral constraints in spectroscopic surveys., v. 2019, n. 8, 036, p. 036, Aug. 2019. Cited 1 time on page [87](#).
- DES COLLABORATION; ABBOTT, T; ALDERING, G, et al. The Dark Energy Survey. [arXiv:astro-ph/0510346](#), Jan. 2005. Cited 3 times on pages [19](#), [45](#).
- DES COLLABORATION; ABBOTT, T M C; ABDALLA, F B; ALARCON, A; ALLAM, S, et al. Dark Energy Survey Year 1 results: measurement of the baryon acoustic oscillation scale in the distribution of galaxies to redshift 1. **Monthly Notices of the Royal Astronomical Society**, Oxford University Press (OUP), v. 483, n. 4, p. 4866–4883, Dec. 2018. Cited 1 time on page [48](#).
- DES COLLABORATION; ABBOTT, T. M. C.; ABDALLA, F. B.; ALARCON, A.; ALEKSIC, J., et al. Dark Energy Survey year 1 results: Cosmological constraints from galaxy clustering and weak lensing. **Phys. Rev. D**, American Physical Society, v. 98, p. 043526, 4 Aug. 2018. Cited 1 time on page [46](#).
- DES COLLABORATION; ABBOTT, T. M. C.; AGUENA, M., et al. **Dark Energy Survey Year 3 Results: A 2.7% measurement of Baryon Acoustic Oscillation distance scale at redshift 0.835**. [S.l.: s.n.], 2021. arXiv: [2107.04646 \[astro-ph.CO\]](#). Cited 15 times on pages [20](#), [52](#), [55](#), [58](#), [62](#), [65](#), [68](#), [69](#), [71](#).
- DJORGOVSKI, S. G. et al. Sky Surveys. In: OSWALT, Terry D. et al. (Eds.). **Planets, Stars and Stellar Systems**. Hardcover. [S.l.]: Springer, Nov. 2013. P. 4290. ISBN 978-9048188529. Cited 1 time on page [28](#).
- DODELSON, Scott. **Modern Cosmology**. Hardcover. [S.l.]: Academic Press, Mar. 2003. P. 456. Cited 2 times on pages [33](#), [39](#).
- DRLICA-WAGNER, A. et al. Dark Energy Survey Year 1 Results: The Photometric Data Set for Cosmology. American Astronomical Society, v. 235, n. 2, p. 33, Apr. 2018. Cited 1 time on page [46](#).
- EFSTATHIOU, G. Myths and truths concerning estimation of power spectra: the case for a hybrid estimator., v. 349, n. 2, p. 603–626, Apr. 2004. Cited 1 time on page [53](#).
- EISENSTEIN, Daniel J.; ANNIS, James, et al. Spectroscopic Target Selection for the Sloan Digital Sky Survey: The Luminous Red Galaxy Sample. American Astronomical Society, v. 122, n. 5, p. 2267–2280, Nov. 2001. Cited 1 time on page [48](#).

- EISENSTEIN, Daniel J.; HU, Wayne. Baryonic Features in the Matter Transfer Function. *American Astronomical Society*, v. 496, n. 2, p. 605–614, Apr. 1998. Cited 1 time on page 39.
- EISENSTEIN, Daniel J.; SEO, Hee-Jong, et al. Improving Cosmological Distance Measurements by Reconstruction of the Baryon Acoustic Peak. *American Astronomical Society*, v. 664, n. 2, p. 675–679, Aug. 2007. Cited 1 time on page 43.
- EISENSTEIN, Daniel J.; WEINBERG, David H., et al. SDSS-III: Massive Spectroscopic Surveys of the Distant Universe, the Milky Way, and Extra-Solar Planetary Systems., v. 142, n. 3, 72, p. 72, Sept. 2011. Cited 1 time on page 19.
- EISENSTEIN, Daniel J.; ZEHAVI, Idit, et al. Detection of the Baryon Acoustic Peak in the Large-Scale Correlation Function of SDSS Luminous Red Galaxies. *American Astronomical Society*, v. 633, n. 2, p. 560–574, Nov. 2005. Cited 1 time on page 19.
- ELLIS, George F. R. Issues in the Philosophy of Cosmology. In: BUTTERFIELD, Jeremy; EARMAN, John (Eds.). **Philosophy of Physics (Handbook of the Philosophy of Science 2)**. Kindle Edition. [S.l.]: North Holland, Nov. 2006. P. 1522. Cited 4 times on page 26.
- FERRERO, I. et al. **Dark Energy Survey Year 3 Results: Galaxy mock catalogs for BAO analysis**. [S.l.: s.n.], 2021. arXiv: [2107.04602 \[astro-ph.CO\]](https://arxiv.org/abs/2107.04602). Cited 4 times on pages 54, 55, 71.
- FLAUGHER, B. et al. THE DARK ENERGY CAMERA. *American Astronomical Society*, v. 150, n. 5, p. 150, Oct. 2015. Cited 1 time on page 46.
- FOREMAN-MACKEY, Daniel et al. emcee: The MCMC Hammer. IOP Publishing, v. 125, n. 925, p. 306–312, Mar. 2013. Cited 1 time on page 62.
- FOSALBA, P. et al. The MICE grand challenge lightcone simulation – I. Dark matter clustering. **Monthly Notices of the Royal Astronomical Society**, v. 448, n. 4, p. 2987–3000, Mar. 2015. ISSN 0035-8711. Cited 2 times on pages 38, 54.
- FREEDMAN, Wendy L.; MADORE, Barry F. The Hubble Constant. **Annual Review of Astronomy and Astrophysics**, v. 48, n. 1, p. 673–710, 2010. Cited 1 time on page 23.
- GARCIA-GARCIA, Carlos; ALONSO, David; BELLINI, Emilio. Disconnected pseudo- C_ℓ covariances for projected large-scale structure data. IOP Publishing, v. 2019, n. 11, p. 043–043, Nov. 2019. Cited 1 time on page 55.
- GATTI, M et al. Dark energy survey year 3 results: weak lensing shape catalogue. **Monthly Notices of the Royal Astronomical Society**, v. 504, n. 3, p. 4312–4336, Apr. 2021. ISSN 0035-8711. Cited 1 time on page 46.

HAMILTON, D. The spectral evolution of galaxies. I. an observational approach., v. 297, p. 371–389, Oct. 1985. Cited 1 time on page 48.

HERBEL, Jorg et al. The redshift distribution of cosmological samples: a forward modeling approach. IOP Publishing, v. 2017, n. 08, p. 035–035, Aug. 2017. DOI: [10.1088/1475-7516/2017/08/035](https://doi.org/10.1088/1475-7516/2017/08/035). Available from: <https://doi.org/10.1088/1475-7516/2017/08/035>. Cited 1 time on page 29.

HERSCHEL, William. XII. On the construction of the heavens. **Philosophical Transactions of the Royal Society of London**, v. 75, p. 213–266, 1785. Cited 0 time on page 24.

HIVON, Eric et al. MASTER of the Cosmic Microwave Background Anisotropy Power Spectrum: A Fast Method for Statistical Analysis of Large and Complex Cosmic Microwave Background Data Sets. **The Astrophysical Journal**, American Astronomical Society, v. 567, n. 1, p. 2–17, Mar. 2002. Cited 3 times on page 53.

HOGG, David W. Distance measures in cosmology. **arXiv:astro-ph/9905116**, May 1999. Cited 2 times on page 37.

HUBBLE, Edwin. A relation between distance and radial velocity among extra-galactic nebulae. **Proceedings of the National Academy of Sciences**, National Academy of Sciences, v. 15, n. 3, p. 168–173, 1929. ISSN 0027-8424. Cited 0 time on page 25.

IZARD, Albert; CROCCE, Martin; FOSALBA, Pablo. ICE-COLA: towards fast and accurate synthetic galaxy catalogues optimizing a quasi-N-body method. **Monthly Notices of the Royal Astronomical Society**, v. 459, n. 3, p. 2327–2341, Apr. 2016. Cited 1 time on page 54.

KNOBEL, Christian. **An Introduction into the Theory of Cosmological Structure Formation**. [S.l.: s.n.], 2013. arXiv: [1208.5931](https://arxiv.org/abs/1208.5931) [astro-ph.CO]. Cited 1 time on page 41.

KRAUSE, Elisabeth; EIFLER, Tim. cosmolike – cosmological likelihood analyses for photometric galaxy surveys. **Monthly Notices of the Royal Astronomical Society**, v. 470, n. 2, p. 2100–2112, May 2017. ISSN 0035-8711. Cited 1 time on page 55.

KURKI-SUONIO, Hannu. **Cosmological Perturbation Theory, Part 1**. [S.l.: s.n.], 2020. Available from: <https://www.mv.helsinki.fi/home/hkurkisu/CosPer.pdf>. Cited 1 time on page 41.

LAHAV, Ofer; CALDER, Lucy; MAYERS, Julian (Eds.). **The Dark Energy Survey: The Story of a Cosmological Experiment**. Hardcover. [S.l.]: WSPC (Europe), Aug. 2020. P. 444. ISBN 978-1786348357. Cited 1 time on page 45.

LAHAV, Ofer; MASSIMI, Michela. Dark energy, paradigm shifts, and the role of evidence. **Astronomy Geophysics**, v. 55, n. 3, p. 3.12–3.15, June 2014. ISSN 1366-8781. Cited 1 time on page 25.

LEAVITT, Henrietta S.; PICKERING, Edward C. Periods of 25 Variable Stars in the Small Magellanic Cloud. **Harvard College Observatory Circular**, v. 173, p. 1–3, Mar. 1912. Cited 1 time on page 23.

LEWIS, Antony; CHALLINOR, Anthony; LASENBY, Anthony. Efficient computation of CMB anisotropies in closed FRW models., v. 538, p. 473–476, 2000. Cited 1 time on page 51.

LONGAIR, Malcolm S. A Brief History of Cosmology. In: FREEDMAN, Wendy (Ed.). **Measuring and modeling the universe**. Cambridge: Cambridge University Press, 2004. Cited 3 times on pages 23, 25.

LOVERDE, M.; AFSHORDI, N. Extended Limber Approximation. **Phys.Rev.D**, v. 78, p. 123506, 2008. Cited 1 time on page 40.

MA, Chung-Pei; BERTSCHINGER, Edmund. Cosmological Perturbation Theory in the Synchronous and Conformal Newtonian Gauges. *American Astronomical Society*, v. 455, p. 7, Dec. 1995. Cited 1 time on page 41.

MASSIMI, Michela. Cosmic Bayes. Datasets and priors in the hunt for dark energy. **European Journal for Philosophy of Science**, v. 11, n. 1, p. 29, Jan. 2021. ISSN 1879-4920. Cited 1 time on page 57.

MUIR, J et al. Blinding multiprobe cosmological experiments. **Monthly Notices of the Royal Astronomical Society**, Oxford University Press (OUP), v. 494, n. 3, p. 4454–4470, Apr. 2020. Cited 1 time on page 30.

NEYRINCK, Mark C.; SZAPUDI, István; SZALAY, Alexander S. Rejuvenating the Matter Power Spectrum: Restoring Information with a Logarithmic Density Mapping., v. 698, n. 2, p. 190–193, June 2009. Cited 1 time on page 30.

PADMANABHAN, Nikhil et al. Calibrating photometric redshifts of luminous red galaxies. **Monthly Notices of the Royal Astronomical Society**, v. 359, n. 1, p. 237–250, May 2005. ISSN 0035-8711. Cited 1 time on page 48.

PEEBLES, P. J. E. Statistical Analysis of Catalogs of Extragalactic Objects. I. Theory., v. 185, p. 413–440, Oct. 1973. Cited 1 time on page 52.

_____. **Cosmology's Century (An Inside History of Our Modern Understanding of the Universe)**. Hardcover. [S.l.]: Princeton University Press, June 2020. P. 440. ISBN 978-0691196022. Cited 2 times on page 27.

PLANCK COLLABORATION et al. Planck 2018 results - VI. Cosmological parameters. **A&A**, v. 641, a6, 2020. Cited 2 times on pages 38, 65.

POSTMAN, Marc; LAUER, Tod R. Brightest Cluster Galaxies as Standard Candles., v. 440, p. 28, Feb. 1995. Cited 1 time on page 48.

ROSS, Ashley J.; BANIK, Nilanjan, et al. Optimized clustering estimators for BAO measurements accounting for significant redshift uncertainty. **Monthly Notices of the Royal Astronomical Society**, v. 472, n. 4, p. 4456–4468, Aug. 2017. ISSN 0035-8711. Cited 1 time on page 48.

ROSS, Ashley J.; PERCIVAL, Will J., et al. The clustering of galaxies in the SDSS-III DR9 Baryon Oscillation Spectroscopic Survey: constraints on primordial non-Gaussianity., v. 428, n. 2, p. 1116–1127, Jan. 2013. Cited 1 time on page 85.

SCHUTZ, Bernard. **A first course in general relativity**. Cambridge New York: Cambridge University Press, 2009. ISBN 978-0521887052. Cited 1 time on page 33.

SEO, Hee-Jong; EISENSTEIN, Daniel J. Probing Dark Energy with Baryonic Acoustic Oscillations from Future Large Galaxy Redshift Surveys. *American Astronomical Society*, v. 598, n. 2, p. 720–740, Dec. 2003. Cited 1 time on page 46.

SEVILLA-NOARBE, I. et al. Dark Energy Survey Year 3 Results: Photometric Data Set for Cosmology. *American Astronomical Society*, v. 254, n. 2, p. 24, May 2021. Cited 0 time on page 47.

SHOJI, Masatoshi; JEONG, Donghui; KOMATSU, Eiichiro. Extracting angular diameter distance and expansion rate of the universe from two-dimensional galaxy power spectrum at high redshifts: baryon acoustic oscillation fitting versus full model. *American Astronomical Society*, v. 693, n. 2, p. 1404–1416, Mar. 2009. Cited 1 time on page 19.

SIDOLI, Nathan Camillo. **History of Modern Physical Sciences - Astronomy in the Long 19th Century: The rise of astrophysics and cosmological speculations**. [S.l.]: Waseda University, 2021. Available from: http://www.astro.yale.edu/vdbosch/astro610_lecture12.pdf. Cited 1 time on page 23.

SOBREIRA, F. et al. Cosmological forecasts from photometric measurements of the angular correlation function. **Phys.Rev.D**, v. 84, p. 103001, 2011. Cited 1 time on page 40.

SPERGEL, D. N. et al. First-Year Wilkinson Microwave Anisotropy Probe (WMAP) Observations: Determination of Cosmological Parameters. *American Astronomical Society*, v. 148, n. 1, p. 175–194, Sept. 2003. Cited 1 time on page 27.

- TAKAHASHI, Ryuichi et al. Revising the halofit model for the nonlinear matter power spectrum. *American Astronomical Society*, v. 761, n. 2, p. 152, Dec. 2012. Cited 1 time on page 51.
- TASSEV, Svetlin; ZALDARRIAGA, Matias. The mildly non-linear regime of structure formation. *IOP Publishing*, v. 2012, n. 04, p. 013–013, Apr. 2012. Cited 1 time on page 54.
- TASSEV, Svetlin; ZALDARRIAGA, Matias; EISENSTEIN, Daniel J. Solving large scale structure in ten easy steps with COLA. *IOP Publishing*, v. 2013, n. 06, p. 036–036, June 2013. Cited 2 times on page 54.
- TEGMARK, Max. How to measure CMB power spectra without losing information. **Phys. Rev. D**, American Physical Society, v. 55, p. 5895–5907, 10 May 1997. Cited 1 time on page 53.
- TROXEL, M. A. et al. Dark Energy Survey Year 1 results: Cosmological constraints from cosmic shear. **Physical Review D**, American Physical Society (APS), v. 98, n. 4, Aug. 2018. Cited 1 time on page 31.
- VLAH, Zvonimir et al. *IOP Publishing*, v. 2016, n. 03, p. 057–057, Mar. 2016. Cited 1 time on page 51.
- WAGNER, C.; MÜLLER, V.; STEINMETZ, M. Constraining dark energy via baryon acoustic oscillations in the (an)isotropic light-cone power spectrum. **A&A**, v. 487, n. 1, p. 63–74, 2008. Cited 1 time on page 19.
- WAKEFIELD, Jon. **Bayesian and frequentist regression methods**. New York, NY: Springer, 2013. ISBN 978-1441909244. Cited 1 time on page 55.
- WANDEL, Benjamin D.; HIVON, Eric; GÓRSKI, Krzysztof M. Cosmic microwave background anisotropy power spectrum statistics for high precision cosmology. **Phys. Rev. D**, American Physical Society, v. 64, p. 083003, 8 Sept. 2001. Cited 1 time on page 53.
- WEINBERG, Steven. **Gravitation and cosmology: principles and applications of the general theory of relativity**. New York: Wiley, 1972. Cited 1 time on page 37.
- XAVIER, Henrique S.; ABDALLA, Filipe B.; JOACHIMI, Benjamin. Improving lognormal models for cosmological fields. **Monthly Notices of the Royal Astronomical Society**, v. 459, n. 4, p. 3693–3710, Apr. 2016. ISSN 0035-8711. Cited 1 time on page 54.
- ZHAN, Hu; TYSON, J Anthony. Cosmology with the Large Synoptic Survey Telescope: an overview. **Reports on Progress in Physics**, IOP Publishing, v. 81, n. 6, p. 066901, Apr. 2018. Cited 1 time on page 48.

ZUNTZ, J. et al. CosmoSIS: Modular cosmological parameter estimation. **Astronomy and Computing**, v. 12, p. 45–59, 2015. ISSN 2213-1337. Cited 1 time on page [51](#).

ZYLA, P.A. et al. Review of Particle Physics. **PTEP**, v. 2020, n. 8, p. 083c01, 2020. DOI: [10.1093/ptep/ptaa104](https://doi.org/10.1093/ptep/ptaa104). Cited 1 time on page [27](#).

Appendix

PRIMORDIAL NON-GAUSSIANITY TEMPLATES AND PRELIMINARY MEASUREMENTS

As we were working with the theory and methods of our main project, we came to realize they could be useful for detecting different features on the power spectrum, as long as the features can be parameterized in a similar way. This conclusion led us to a parallel work with a small group on the DES collaboration investigating primordial non-gaussianities.

A.1 CONCEPT

The detection of primordial non-Gaussianities (PNGs) on density fluctuations is an important probe for inflationary models. If a Gaussian field can be ruled out, more complex, multiple-field inflation scenarios are favored (BARREIRA, 2020; ALVAREZ et al., 2014). We worked in collaboration with Dr. Santiago Avila (UAM) and Dr. Hugo Camacho (IFT-UNESP) to develop ways of using the DES-BAO methodology for constraining PNG parameters from the BAO sample.

A.2 FORMALISM

A.2.1 PNG parametrization for the angular power spectra

Primordial non-Gaussianity is usually parametrized by a parameter called f_{NL} , which measures the departure of the observable in respect to a Gaussian model. In order to constrain PNG from galaxy distribution, we use the galaxy bias, modeling a scale-dependent contribution in addition to the linear bias. Eq. A.1 was proposed as our initial bias model, based on the model by Ross, Percival, et al. (2013).

$$b(k) = b_g + f_{NL}(b_g - 1)M(k, z), \quad (\text{A.1})$$

where

$$M(k, z) = \frac{3(1.3)\delta_c\Omega_{tot}}{k^2(H/c)^2T(k)D(z)}, \quad (\text{A.2})$$

and $D(z)$ is the linear growth function.

Our APS modeling was repeated, with additional RSD terms and the scale-dependent bias.

$$C_\ell^{ab} = \frac{2}{\pi} \int z_1 z_2 k k^2 P_{ab}(k, z_1, z_2) \Delta_\ell^a(k, z_1) \Delta_\ell^b(k, z_2), \quad (\text{A.3})$$

$$\Delta_\ell = \Delta_\ell^D + \Delta_\ell^{\text{RSD}} + \Delta_\ell^{\text{PNG}}. \quad (\text{A.4})$$

We take Eq. 2.44 and add an additional projection kernel to account for redshift-space distortions.

$$C_\ell = \int dk k^2 P(k, z=0) [b_g \Psi_\ell(k) + \Psi_\ell^{\text{RSD}}(k)]^2, \quad (\text{A.5})$$

The effect of the new term for a scale-dependent bias will be that of a new projection kernel.

$$C_\ell = \int dk k^2 P(k) [b_g \Psi_\ell(k) + f_{NL}(b_g - 1) \Psi_\ell^M(k) + \Psi_\ell^{\text{RSD}}(k)]^2, \quad (\text{A.6})$$

where

$$\Psi_\ell(k) = \sqrt{\frac{2}{\pi}} \int dz n(z) M(k, z) j_\ell(kr(z)). \quad (\text{A.7})$$

Since each integral from Eq. (A.6) is independent from the linear bias and the f_{NL} parameter, we can rewrite the whole equation in terms of six C_ℓ templates, which can be computed before parameter fitting.

$$\begin{aligned} C_\ell &= b_g^2 \int dk k^2 P(k) [\Psi_\ell(k)]^2 \\ &+ \int dk k^2 P(k) [\Psi_\ell^{\text{RSD}}(k)]^2 + 2b_g \int dk k^2 P(k) \Psi_\ell(k) \Psi_\ell^{\text{RSD}}(k) \\ &+ f_{NL}^2 (b_g - 1)^2 \int dk k^2 P(k) [\Psi_\ell^M(k)]^2 + 2b_g f_{NL} (b_g - 1) \int dk k^2 P(k) \Psi_\ell(k) \Psi_\ell^M(k) \\ &+ 2f_{NL} (b_g - 1) \int dk k^2 P(k) \Psi_\ell^{\text{RSD}}(k) \Psi_\ell^M(k). \end{aligned} \quad (\text{A.8})$$

$$\begin{aligned} \Rightarrow C_\ell &= b_g^2 C_\ell^{\delta\delta} + C_\ell^{\text{RSD RSD}} + 2b_g C_\ell^{\delta\text{RSD}} \\ &+ f_{NL}^2 (b_g - 1)^2 C_\ell^{\text{PNG PNG}} + 2b_g f_{NL} (b_g - 1) C_\ell^{\delta\text{PNG}} + 2f_{NL} (b_g - 1) C_\ell^{\text{RSD PNG}}. \end{aligned} \quad (\text{A.9})$$

A.2.1.1 A simplified model

For an initial simplified model, we ignored the terms related to redshift space distortions and used Limber approximation on the remaining terms. These simplifications leave us with (A.10), which has only three terms.

$$\begin{aligned}
C_\ell = & b_g^2 \int dz H(z) \left[\frac{n(z)}{r} \right]^2 P \left(z, \frac{l+1/2}{r} \right) \\
& + 2b_g f_{NL} (b_g - 1) \int dz H(z) \left[\frac{n(z)}{r} \right]^2 M \left(z, \frac{l+1/2}{r} \right) P \left(z, \frac{l+1/2}{r} \right) \\
& + f_{NL}^2 (b_g - 1)^2 \int dz H(z) \left[\frac{n(z)}{r} \right]^2 M^2 \left(z, \frac{l+1/2}{r} \right) P \left(z, \frac{l+1/2}{r} \right).
\end{aligned} \tag{A.10}$$

A.3 PRELIMINARY RESULTS

With our model in hands, we followed the same methodology from our main project with equation A.10 being our template. Initial MLE fits for the set of 1952 COLA mocks were performed, yielding the distribution found on Figure A.1. The unexpected bimodal feature shows there is still more to improve in our model. The following steps of the project will include the incorporation of integral constraint parameters, as done by [de Mattia and Ruhlmann-Kleider \(2019\)](#).

We also ran MCMC chains for different cuts at large scales, to test how much they impact the sampled values. Figure A.2 shows our results. Each removed large scale ℓ bin increases significantly the $_{NL}$ parameter distribution. This means these scales should be considered carefully on the upcoming analysis.

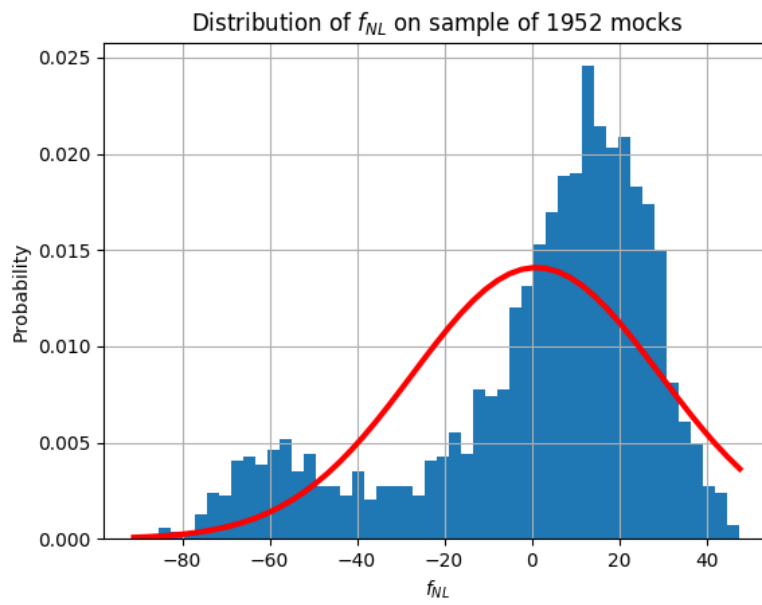


Figure A.1 – Fitted f_{NL} parameter distribution on the COLA mocks.

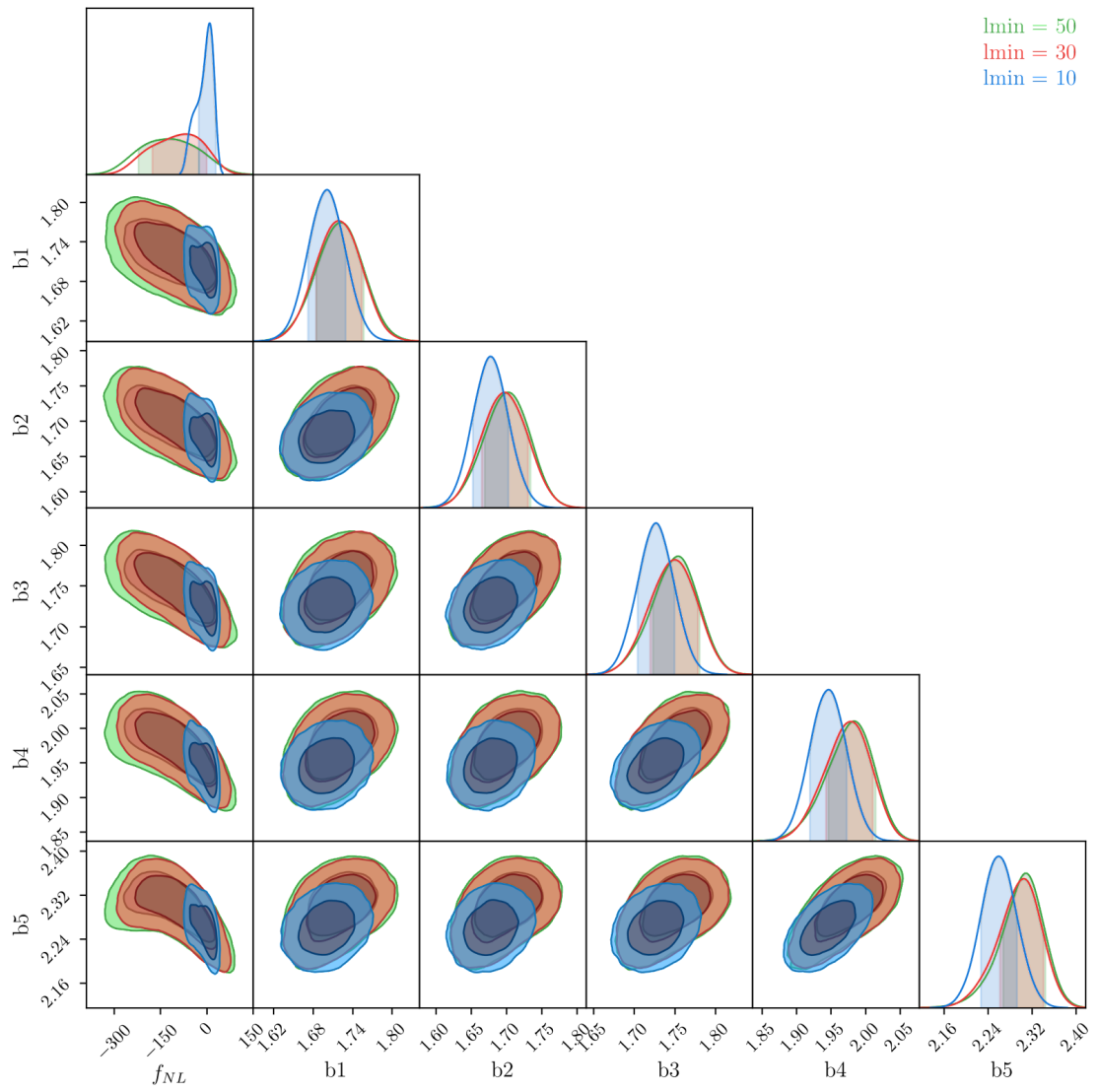


Figure A.2 – Sampled f_{NL} and bias parameters for different scale cuts.

APPENDIX B

TABLE OF PARAMETERS FOR Y3 MEASUREMENTS

z bin	Parameter	MLE	MCMC
-	α	0.950 ± 0.031	$0.961^{+0.029}_{-0.028}$
1	B	0.97 ± 0.30	$0.93^{+0.31}_{-0.30}$
	$A_{-1} \times 10^3$	0.34 ± 0.34	$0.53^{+0.35}_{-0.34}$
	$A_0 \times 10^5$	3.0 ± 3.1	$-3.7^{+3.1}_{-3.3}$
	$A_1 \times 10^9$	-19 ± 16	9^{+16}_{-16}
	$A_2 \times 10^{12}$	30 ± 21	-7^{+21}_{-22}
2	B	1.15 ± 0.25	$0.99^{+0.24}_{-0.25}$
	$A_{-1} \times 10^3$	0.03 ± 0.20	$0.32^{+0.20}_{-0.20}$
	$A_0 \times 10^5$	1.4 ± 1.8	$-2.6^{+1.9}_{-1.8}$
	$A_1 \times 10^9$	-4.7 ± 7.8	$6.3^{+7.9}_{-8.1}$
	$A_2 \times 10^{12}$	5.4 ± 9.2	$-5.0^{+9.6}_{-9.4}$
3	B	1.02 ± 0.21	$1.02^{+0.22}_{-0.21}$
	$A_{-1} \times 10^3$	0.18 ± 0.14	$0.24^{+0.14}_{-0.14}$
	$A_0 \times 10^5$	0.2 ± 1.3	$-2.0^{+1.4}_{-1.4}$
	$A_1 \times 10^9$	-2.7 ± 5.3	$4.8^{+5.4}_{-5.5}$
	$A_2 \times 10^{12}$	4.8 ± 5.8	$-3.7^{+6.0}_{-5.8}$
4	B	1.08 ± 0.20	$1.01^{+0.20}_{-0.20}$
	$A_{-1} \times 10^3$	0.15 ± 0.12	$0.22^{+0.12}_{-0.12}$
	$A_0 \times 10^5$	-0.8 ± 1.3	$-1.7^{+1.4}_{-1.4}$
	$A_1 \times 10^9$	1.9 ± 4.8	$3.9^{+5.2}_{-5.1}$
	$A_2 \times 10^{12}$	-0.9 ± 4.9	$-2.9^{+5.2}_{-5.3}$
5	B	1.26 ± 0.19	$1.06^{+0.19}_{-0.19}$
	$A_{-1} \times 10^3$	0.12 ± 0.10	$0.17^{+0.10}_{-0.10}$
	$A_0 \times 10^5$	-2.4 ± 1.1	$-1.3^{+1.2}_{-1.2}$
	$A_1 \times 10^9$	7.8 ± 3.9	$3.0^{+4.1}_{-4.0}$
	$A_2 \times 10^{12}$	-6.7 ± 3.6	$-2.1^{+3.8}_{-3.8}$

Table B.1 – Value of all 26 parameters for MLE and MCMC fits with DES Y3 data.